Stepped-Frequency Binary Offset Carrier Modulation for Global Navigation Satellite Systems

Seung-Hyun Kong*, *Senior Member, IEEE*, Sangjae Cho, Taeseon Kim, and Sanguk Lee

***Abstract*—In this paper, we propose Stepped-Frequency Binary Offset Carrier (SFBOC) modulation for Global Navigation Satellite Systems (GNSS) that use spread spectrum signals. SFBOC modulation generates a Binary Offset Carrier (BOC) signal of which the subcarrier frequency varies stepwise within each period of the pseudorandom-noise (PRN) code. The generated SFBOC signal can have a sharp autocorrelation function (ACF) output and an almost flat spectrum over a wide frequency band. These characteristics result in correlation properties, multipath mitigation, and anti-interference that are superior to those of conventional GNSS modulations. To testify, we compare the performance of SFBOC in various aspects to conventional GNSS modulations and other time-varying subcarrier frequency (TVSF) modulations. From numerical simulations, we show that the proposed SFBOC has higher ranging accuracy, lower tracking ambiguity, and more robustness to noise, interference, and multipath than the conventional GNSS modulations. In addition, we demonstrate that the proposed SFBOC moulation has two advantages while other modulations with TVSF cannot have both; that SFBOC is robust to code-Doppler and that, when filterbank is employed, SFBOC improves the signal-to-noise ratio (SNR) significantly without any loss of weak early arrival path in the Non-line of sight (NLOS) multipath environments.**

***Index Terms*—GNSS, SFCW, BOC, TVSF.**

I. Introduction

Global Navigation Satellite Systems (GNSS), such as Global Positioning System (GPS), Galileo, BeiDou Navigation Satellite System (BDS), Quasi-Zenith Satellite System (QZSS), and Indian Regional Navigational Satellite System (IRNSS), use various Binary Offset Carrier (BOC) modulations (hereinafter referred to as BOC) to minimize interference between spread spectrum signals sharing the same frequency band and to improve the ranging accuracy of the receiver [1]–[4]. BOC modulation splits the spectrum of the Binary Phase Shift Key (BPSK) signal into upper and lower images at positive and negative BOC subcarrier frequencies, respectively. [3]–[6]

BOC is expressed as BOC(m,n), where n represents the Chip duration $T_c(T_c = T_0/n)$ and m expresses the subcarrier period T_{sc} ($T_{sc} = T_0/m$), where $T_0 = 10^{-3}/1023$ [s] is the GPS L1 frequency coarse acquisition (C/A) code chip duration, and m and n are positive integers. In BPSK modulation (hereinafter referred to as BPSK), the main lobe of the Autocorrelation Function (ACF) output has only one triangular peak, whereas BOC(m,n) has $2(2m/n - 1))$ side peaks [3], [7] within $[-T_c, T_c]$. The side peaks in the ACF output cause ambiguity in detecting and tracking the time delay of the first-arrival path (FP) in the GNSS receiver, and can be a source of ranging errors in multipath channels [8]–[15]. Future GNSS requires signals with a sharp ACF output main lobe and low side peaks to improve positioning performance in multipath channels [5], [16] and, at the same time, demands lower interference to the conventional GNSS signals. However, as the GNSS band becomes increasingly crowded, it is becoming increasingly difficult for a new GNSS signal to be used in the same frequency band [17], [18].

In [19]–[21], modulations with time-varying subcarrier frequen (TVSF) are introduced to reduce both the interference to signals sharing the same band and ambiguity of ACF output side peaks using special modulation techniques that vary the BOC subcarrier frequency $f_{sc}(= 1/T_{sc})$ over time. In [20], similar to Linear Frequency Modulated (LFM), Generalized BOC (GBOC) modulation (hereinafter referred to as GBOC) varies the subcarrier frequency linearly and continuously from $1 \times f_0(= 1/T_0)$ to $m \times f_0$ during each chip period T_c. GBOC shows a very sharp ACF output and high anti-interference performance, however, GBOC has a much wider null-to-null Bandwidth (BW) than that of BOC(m, n), $2f_0(m+n)$. In [21], Frequency-Hopping BOC (FHBOC) modulation (hereinafter referred to as FHBOC) is proposed, where the BOC subcarrier frequency f_{sc} is hopping according to a pseudorandom-noise (PRN) sequence. However, in FHBOC, since the frequency hopping period is multiple times longer than the spreading code period, the acquisition complexity increases multiple times.

In this paper, we propose a new TVSF modulation, Stepped-Frequency Binary Offset Carrier (SFBOC) modulation (hereinafter referred to as SFBOC), that is based on stepped-frequency continuous wave (SFCW) [22], [23] for spread spectrum GNSS signals. SFBOC has a varying discrete BOC subcarrier frequencies eith equal frequency distance, such that BOC subcarrier frequency decreases (or increases) stepwise during the spreading code period T_{code}. The proposed SFBOC is a new satellite navigation signal developed for Korea Positioning System (KPS) in a research with Electronics and Telecommunications Research Institute (ETRI), and can be considered as an advanced future GNSS signal. The proposed SFBOC has several distinguished advantages compared to other modulations with TVSF such as GBOC and FHBOC. First, (similar to FHBOC) SFBOC has a narrower null-to-null bandwidth than GBOC even when the highest subcarrier frequency mf_0 of SFBOC is the same to GBOC. Second, (sim-

*Corresponding author (e-mail: skong@kaist.ac.kr)

Seung-Hyun Kong, Sangjae Cho, and Taeseon Kim are with Graduate School of Mobility, Korea Advanced Institute of Science and Technology, Daejeon, Korea, 340-51 (e-mail: {sanje, ktset}@kaist.ac.kr)

Sanguk Lee is with KPS satellite navigation research center, Electronics Telecommunications Research Institute, Daejeon, Korea, 341-30 (e-mail: slee@etri.re.kr)

ilar to FHBOC) SFBOC is more robust to the code Doppler and sampling timing offset (STO) than GBOC, because of the longer frequency dwelling time. Third, SFBOC has the same acquisition complexity to the conventional BOC, since SFBOC has a deterministic and slow subcarrier frequency hopping pattern. On the contrary, FHBOC has acquisition complexity increasing with the length of the subcarrier frequency hopping period. Finally, when a single-sideband processing-based filterbank (SBPFB) is employed to significantly improve the signal-to-noise ratio (SNR) of TVSF signals, FHBOC may suffer severely from blanking weak FP signal in the Non-line of sight (NLOS) multipath channels, which results in a degraded FP detection performance. However, the weak FP blanking can be neglected in the SFBOC and there is no performance degradation in the FP detection in NLOS multipath channels. We may summarize the contributions of this paper as follows.

- We propose SFBOC, which has a discrete and stepwise time-varying BOC subcarrier frequency. We demonstrate the superiority of the SFBOC performance in various aspects with the conventional GNSS modulation and other modulations with TVSF.
- We introduce SBPFB to distinguish SFBOC and FHBOC, which significantly improves the SNR of the received signals with modulations with TVSF, but FHBOC suffers from the loss of weak earlier arrival signals when filterbank is employed in NLOS multipath channels.

The rest of this paper is organized as follows. Section II introduces the proposed SFBOC and the modulation parameters. Section III compares the simulation results for various performance aspects defined in Table I to demonstrate that the proposed SFBOC is superior to the conventional GNSS modulations and modulations with TVSF, while it requires a low implementation complexity similar to the conventional GNSS modulations. In Section IV, we introduce SBPFB that significantly increases the SNR for SFBOC and FHBOC, and we show that SFBOC does not suffer from the blanking of weak earlier arrival signals as FHBOC does, when SBPFB is implemented. Section V draws the conclusion of this paper, and Appendix introduces additional simulation results that are not explained in detail in the main body of the paper.

II. STEPPED-FREQUENCY BINARY OFFSET CARRIER (SFBOC) MODULATION

In this section, mathematical expressions and parameters for the proposed SFBOC are introduced. And we derive ACF outputs and Power Spectrum Density (PSD) [24] for different SFBOC parameters. Based on the analysis, we discuss the best-performing parameters of the SFBOC for a given limited frequency band. Note that comparison with other TVSFs that have similar characteristics to SFBOC is introduced in Section III.

A. Proposed SFBOC

The proposed SFBOC consists of various BOCs over time. The general expression of a BOC signal $y_{BOC,R}(t)$ with carrier frequency f_r can be found as

$$y_{BOC,R}(t) = D(t)C(t)p_{BOC}(t)\cos(2\pi f_r t), \tag{1}$$

where $D(t)$ is the navigation data signal,

$$C(t) = \sum_{k=0}^{N-1} C_k \Pi\left(\frac{t - kT_c}{T_c} - \frac{1}{2}\right), \tag{2}$$

$$p_{BOC}(t) = \text{sign}\left[\sin\left(2\pi f_{sc} t + \theta_{BOC}\right)\right], \tag{3}$$

$$\Pi(t) = \begin{cases} 1, & -\frac{1}{2} \le t \le \frac{1}{2} \\ 0, & \text{otherwise} \end{cases} \tag{4}$$

C_k is the k-th chip of the pseudorandom-noise (PRN) code sequence of N code chips with a chip rate f_c, chip width T_c, and PRN code sequence period T_{code}, $\Pi(t)$ is a rectangular function, $p_{BOC}(t)$ is a BOC(m,n) subcarrier with a subcarrier frequency $f_{sc} = mf_0 (= 1/T_{sc})$, and f_r is the carrier frequency. Note that $p_{BOC}(t)$ can be either sine-phased ($\theta_{BOC} = 0$) or cosine-phased ($\theta_{BOC} = \pi/2$) BOC subcarrier depending on θ_{BOC}. In the relatively long interval of a navigation data bit (e.g., $T_b = 20[\text{ms}]$), D(t) has a constant value of either -1 or 1. In this paper, we assume that $p_{BOC}(t)$ is the sine-phased BOC subcarrier (i.e., $\theta_{BOC} = 0$), which has been widely-used in GNSS, and that $D(t)$ is assumed to be 1 for mathematical simplicity in the expressions. Therefore, the baseband signal of (1) can be simplified to

$$y_{BOC}(t) = C(t)p_{BOC}(t). \tag{5}$$

The proposed SFBOC has a stepwise decreasing (or increasing) subcarrier frequency within every T_{code}. The SFBOC TVSF can be written as

$$f_{sc}(t) = M_k(t) \times f_0, \tag{6}$$

where

$$M_k(t) = m_k \times \Pi\left(\frac{N_M}{T_{\text{code}}} t - k - \frac{1}{2}\right), \tag{7}$$

Suppose that the minimum and maximum possible m_k in a given frequency bandwidth are m_l and m_h, respectively, such that $m_l f_0$ and $m_h f_0$ are the lowest and the highest BOC subcarrier frequencies within the given bandwidth, respectively, then we find

$$m_k = \begin{cases} m_l + k i_m, & \text{for increasing } M_k(t) \\ m_h - k i_m, & \text{for decreasing } M_k(t) \end{cases} \tag{8}$$

where i_m is the frequency step size and $k = 0, 1, 2, \ldots (N_{M-1})$, and the total number of subcarrier frequencies per T_{code} is

$$N_M = (m_h - m_l)/i_m + 1. \tag{9}$$

As shown in (7) and (8), $M_k(t)$ is fixed during the frequency dwelling time,

$$T_M = \frac{T_{code}}{N_M}, \tag{10}$$

and $M_k(t)$ decreases (or increases) stepwise as k (8) decreases (or increases) from 0 to $N_M - 1$. The performances of the SFBOC with the increasing $M_k(t)$ and decreasing $M_k(t)$ are almost the same, but decreasing $M_k(t)$ is slightly more robust to the code Doppler (see Appendix E). Therefore, in the following, we assume that the proposed SFBOC has the decreasing $M_k(t)$, and SFBOC with m_k decreasing from m_h

TABLE I
PERFORMANCE EVALUATION LIST.

Aspects	Simulations	GBOC [20]	FHBOC [21]	SFBOC
Correlation Property	Zero Crossings Nearest the Main peak (ZCNM)		√	√
	ACF main-peak-to-maximum-side-peak ratio (MSR)		√	√
Spectrum Property	Fractional out-of-band power(FOBP)	√		√
Ranging Accuracy	Gabor bandwidth(GB)	√	√	√
Tracking anti-ambiguity	S-curve		√	√
	Tracking discriminator gain	√		√
White noise mitigation	Tracking error variance for AWGN channel	√	√	√
Multipath mitigation	Multipath Error Envelope (MEE)	√	√	√
Interference mitigation	Spectral Separation Coefficient (SSC)		√	√
	Processing gain (PG) in narrow band	√	√	√
Doppler mitigation	Correlation loss according to doppler frequency	√		√
Receiver complexity	Bandwidth requirement			√
	Search space		√	√
	Single-sideband Processing-based Filterbank(SBPFB)			√

to m_l by $-i_m$ is expressed as SFBOC(m_h:$-i_m$:m_l,n), and the baseband SFBOC signal can be found as

$$\begin{aligned} y_{SF}(t) &= C(t)p_{SF}(t) \\ &= C(t)\,\mathrm{sign}\left[\sin\left(2\pi M_k(t)f_0 t\right)\right], \end{aligned} \tag{11}$$

where $p_{SF}(t)$ is the SFBOC subcarrier.

Fig. 1 is a block diagram for the SFBOC modulation process. Except for the frequency multiplier in SFBOC Waveform Generator Block, where time-varying BOC subcarrier frequency $M_k(t)f_0$ is generated, the process is the same to the BOC modulation process [3], [4], [6]. Accordingly, a SFBOC receiver may have a similar processing chain to BOC receivers. More details is discussed in subsection III-G.

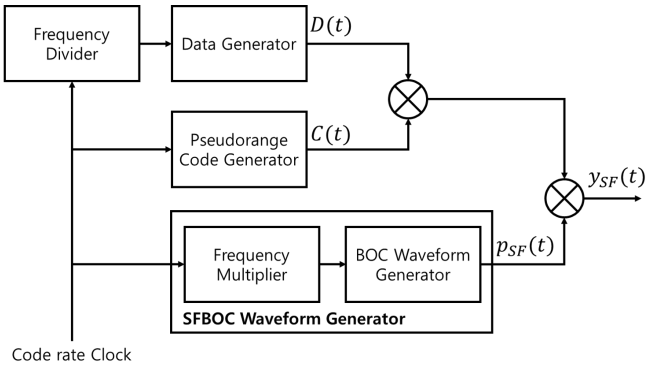

Fig. 1. Block diagram of SFBOC Signal generation.

Note that the SFBOC waveform depends on the parameters m_l, m_h, i_m, and n. For the fixed m_l, higher m_h leads to a better correlation property due to the wider bandwidth of the overall signal during T_{code} [19]–[21], however, this may require a better receiver frequency oscillator [25]. Since the spectrum of SFBOC loses uniform distribution as i_m increases above 2, we consider various m_h and $i_m = 1$ or 2 for $m_l = 1$ in the following analysis.

B. Autocorrelation Property

For SFBOC, the ACF output shape and the power spectral density (PSD) depend on the various parameters such as m_h, i_m, and m_l. The ACF output of SFBOC, $R_{SF}(\tau)$, can be expresses as

$$\begin{aligned} R_{SF}(\tau) &= E\left[y_{SF}(t)y_{SF}^*(t+\tau)\right] \\ &= \mathrm{E}\left[\sum_{l=-\infty}^{+\infty} C_l p_{SF}\left(t-lT_c\right)\right. \\ &\qquad \left.\sum_{u=-\infty}^{+\infty} C_u^* p_{SF}^*\left(t+\tau-uT_c\right)\right], \end{aligned} \tag{12}$$

where C_l (or C_u) is defined in (2) and $p_{SF}(t)$ is defined in (11). Since BOC(m_k, 1) (for $k = 0, 1, \ldots, N_{M-1}$) is uniformly (i.e., evenly) distributed within T_{code} in SFBOC(m_h:$-i_m$:m_l,1), we can express $R_{SF}(\tau)$ referring to [17], [26] as

$$\begin{aligned} R_{SF}(\tau) &= \frac{1}{N_M}\sum_{k=0}^{N_M-1}\left(\sum_{l=-\infty}^{+\infty} C_l\,\mathrm{sign}\left[\sin\left(2\pi M_k\left(t-lT_c\right)f_0\right)\right]\right. \\ &\qquad \left.\sum_{u=-\infty}^{+\infty} C_u^*\,\mathrm{sign}\left[\sin\left(2\pi M_k\left(t+\tau-uT_c\right)f_0\right)\right]\right) \\ &\cong \frac{1}{N_M}\sum_{k=0}^{N_M-1} R_{BOC(m_k,n)}(\tau), \end{aligned} \tag{13}$$

where

$$\begin{aligned} R_{BOC(m_k,n)}(\tau) = R_{\frac{T_0}{m_k}}(\tau) + &\sum_{i=1}^{\frac{2m_k}{n}-1}(-1)^i\left(1-\frac{in}{2m_k}\right) \\ &\times R_{\frac{T_0}{2m_k}}\left(|\tau|-\frac{kT_0}{2m_k}\right), \end{aligned} \tag{14}$$

$$R_L(t) \triangleq \begin{cases} 1 - \frac{|t|}{L}, & |t| \le L \\ 0, & \text{otherwise} \end{cases}. \tag{15}$$

The main lobe of the ACF output should be sharp and the magnitude of the side peaks should be small [26]–[28] for higher ranging accuracy and robustness against multipath. In Fig.2a, various $R_{SF}(\tau)$ (12) are compared; SFBOC(3:-2:1,1) has relatively large $i_m(=2)$ and small $m_h(=3)$, which results in the width of ACF output main lobe of about $0.3T_c$ and large side peaks. On the other hand, SFBOC(11:-1:1,1) has the best correlation property among ACF outputs shown in Fig. 2a, because of the narrow main lobe of width about $0.05T_c$ and the smallest side peaks of magnitudes less than 0.2. Note that for all cases with $i_m = 2$, side peaks have large magnitudes and that for large m_h and $i_m = 1$, the generated SFBOC has an excellent ACF output shape. We compare $R_{SF}(\tau)$ (13) for $m_h = \{3, 4, \dots 8\}$ and $i_m = m_l = n = 1$ in Fig. 2b, where only single side ACF outputs (i.e., $0 \le \tau < 0.5T_c$) are illustrated. As expected, larger m_h results in a sharper main lobe and smaller side peak magnitudes.

We compare ACF outputs of the proposed SFBOC with $n = 1$ to the conventional GNSS modulations, such as BPSK(1), BOC(1,1), BOC(6,1), and CBOC(6,1,1/11), with the same chip rate $1 \times f_0$ (= 1.023MHz, i.e., $n = 1$) on service in L1 band. Note that the null-to-null bandwidth of SFBOC(6:-1:1,1) is comparable to BOC(6,1) and CBOC(6,1,1/11). Fig. 3a and Fig. 3b show the main lobes of ACF outputs from $[-1, 1]T_c$ and $[0, 0.3]T_c$, respectively. Notice that CBOC(6,1,1/11) has a much wider ACF output main lobe but much smaller side peak magnitudes than BOC(6,1). However, the ACF output main lobe of the SFBOC(6:-1:1,1) is slightly wider than BOC(6,1) but significantly narrower than CBOC(6,1,1/11). In addition, the side peak magnitudes of the SFBOC(6:-1:1,1) are much smaller than those of BOC(6,1) and CBOC(6,1,1/11). FHBOC and GBOC have the same and similar ACF output to SFBOC, respectively, as shown in Appendix A. For further comparison, Appendix A introduces numerical analysis of the Zero crossings nearest the main peak (ZCNM) and ACF main-peak-to-maximum-side-peak ratio (MSR).

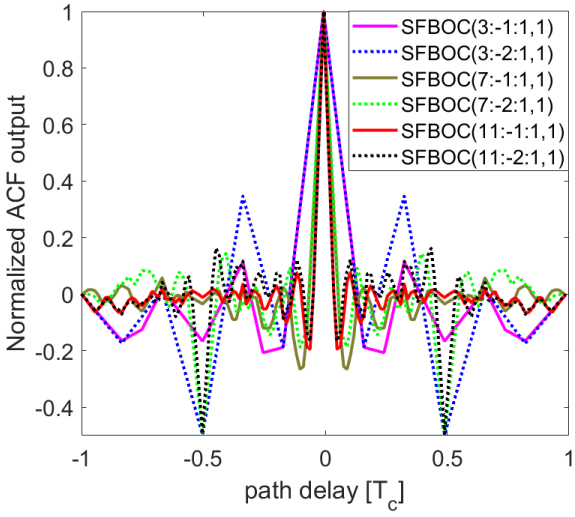

(a) ACF output for various parameters

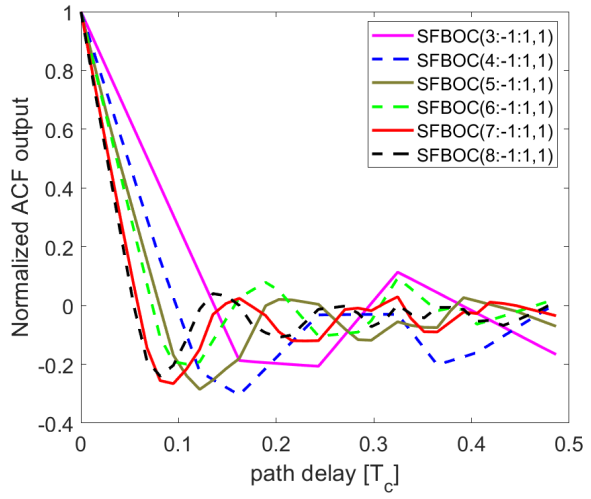

(b) ACF output for $i_m = 1$

Fig. 2. Normalized ACF outputs of SFBOC.

C. Power Spectrum

Based on the Wiener–Khinchin theorem [29], Power Spectral Density (PSD) can be derived through the Fourier transform of the ACF output. Since the proposed SFBOC includes several BOCs during one code period and assuming BOC(m, n) signals with different m have negligible cross-correlation, the PSD $G_{SF}(f)$ (16) of the SFBOC can be found using the PSD $G_{BOC}(f)$(17) [4] of the BOC as

$$G_{SF}(f) = \frac{1}{N_M} \sum_{k=0}^{N_M-1} G_{BOC(m_k,1)}(f), \tag{16}$$

where

$$\begin{aligned} G_{BOC(m_k,1)}(f) &= \mathcal{F}\left\{R_{BOC_{(m_k,1)}}(\tau)\right\} \\ &= f_c \left[\frac{\sin\left(\frac{\pi f}{f_0}\right)\sin\left(\frac{\pi f}{2m_k f_0}\right)}{\pi f \cos\left(\frac{\pi f}{2m_k f_0}\right)}\right]^2, \end{aligned} \tag{17}$$

and $R_{BOC_{(m_k,1)}}(\tau)$, and $G_{BOC(m_k,1)}(f)$ indicate the ACF output and PSD of the $BOC(m_k, 1)$, respectively. Since SFBOC is a modulation that consists of BOCs of N_M different frequencies, SFBOC(6:-1:1,1) can be found as the average PSD of multiple BOCs as shown in Fig. 4.

Fig. 5 compares PSDs of various m_h and i_m for SFBOC(m_h:$-i_m$:1,1). As shown, SFBOC of larger m_h occupies wider spectrum with lower density, and vice versa. Therefore we can expect that SFBOC with larger m_h can have a narrower ACF main lobe. On the other hand, when $i_m > 1$, the separation between the neighboring BOC spectrums becomes too large so that the overall SFBOC spectrum envelope cannot be assumed flat and the magnitudes of ACF side lobes become large as shown in 2a, which may be not useful for multipath mitigation. Therefore, SFBOC with large m_h and $i_m = 1$ has better anti-interference performance than the conventional GNSS modulations [18], [24].

In this section, we introduce SFBOC and show its character-

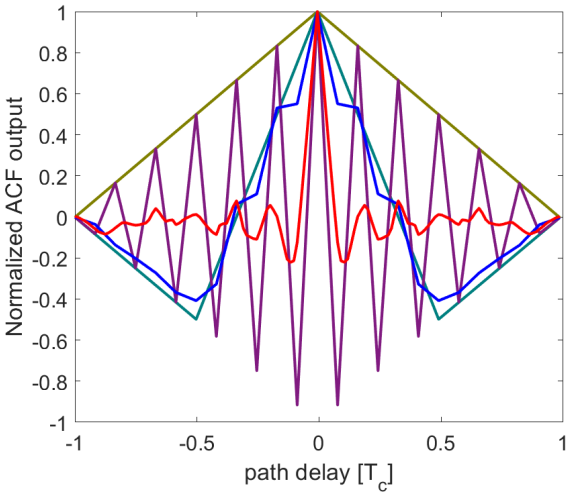

(a) ACF outputs

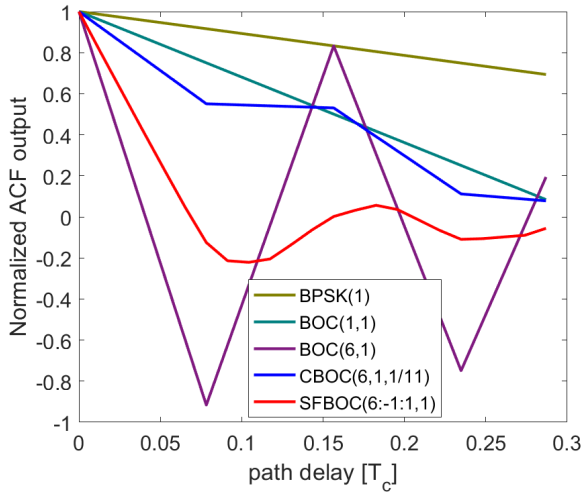

(b) Zoom of ACF outputs

Fig. 3. Normalized ACF outputs of the conventional GNSS modulations and SFBOC(6:-1:1,1).

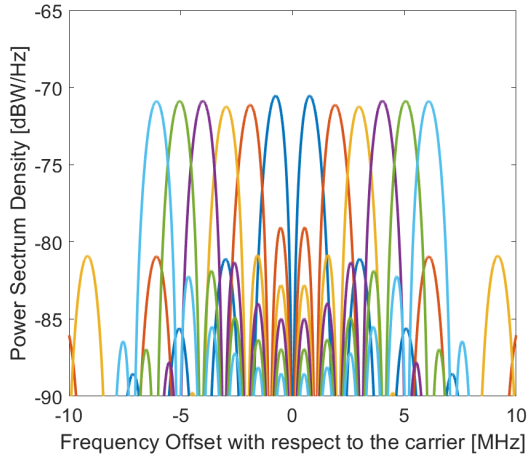

Fig. 4. PSDs for each BOC modulation consisting SFBOC(6:-1:1,1).

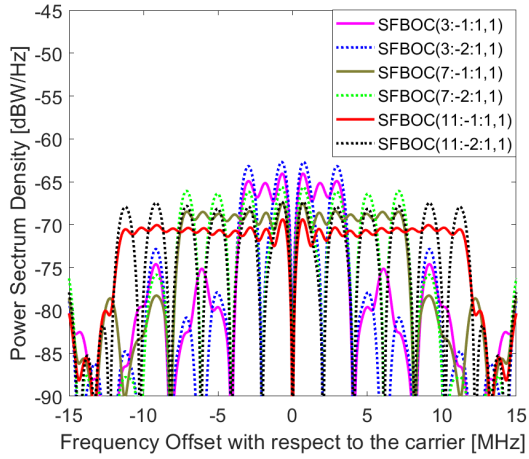

Fig. 5. PSDs of SFBOCs.

istics through the comparison with conventional GNSS modulations. In the next section, we demonstrate the superiority of SFBOC by evaluating the difference from TVSF modulations (GBOC, FHBOC) and performance from various perspectives.

III. PERFORMANCE EVALUATION

In this section, we demonstrate the superiority of SFBOC to conventional GNSS modulations (BPSK(1), BOC(1,1), BOC(6,1), CBOC(6,1,1/11)), and modulations with TVSF (GBOC(6,1,0) [20], FHBOC(6:1:1,1) [21]) for various performance aspects listed in Table I. From this section, we refer to the conventional GNSS modulations and modulations with TVSF as all compared modulations. In subsection III-A, we introduce GBOC [20] and FHBOC [21] and discuss their difference from SFBOC. We analyze PSDs of SFBOC and all compared modulations and compare the anti-interference performance of modulation by analyzing Spectral Separation Coefficient (SSC) [30] and processing gain in subsection III-B, and we compare ranging accuracy based on Gabor bandwidth in subsection III-C. We analyze the code tracking error variance for Additive White Gaussian Noise (AWGN) channel in subsection III-D, and we investigate Multipath Error Envelope (MEE) [31] based on the EL discriminator response (i.e., S-curve) to compare noise robustness and multipath mitigation performance in subsection III-E.

A. Comparison to FHBOC and GBOC

GBOC can be viewed as a BOC with a chirp subcarrier, and the baseband signal modulated with GBOC(m,n,a) [20] can be expressed as

$$y_{GB}(t) = C(t) \sum_{k=0}^{N-1} p_{GB}\left(t - kT_c\right), \tag{18}$$

where

$$p_{GB}(t) = \text{sign}[\sin(\phi(t)], \tag{19}$$

$$\phi(t) = \frac{2m\pi}{n}\left(a\left(\frac{t}{T_c}\right) + (1-a)\left(\frac{t}{T_c}\right)^2\right), 0 \le t \le T_c. \tag{20}$$

As shown in (18), GBOC continuously increases the subcarrier frequency within the chip interval T_c using time-varying $\phi(t)$ (20) [20], and the rate of frequency change depends on the parameter a. In the following analysis, we set $a = 0$ as it shows the best performance in [20].

FHBOC [21] has discrete subcarrier frequency, within the frequency dwelling time less than T_c, that varies pseudo-randomly, and is expressed as FHBOC(m_h:i_m:m_l,n), where $\{m_h{:}i_m{:}m_l\}$ is hopset of pseudorandom hopping frequency indices from the highest to lowest subcarrier frequencies; m_h, i_m, and m_l are respectively the highest m (such that maximum subcarrier frequency $f_h = m_h \times f_0$), the unit of frequency hopping step, and the lowest m (such that minimum subcarrier frequency $f_l = m_l \times f_0$). Note that a clear difference of FHBOC from SFBOC is that while SFBOC has a step-wise slow linear frequency change, FHBOC has a fast and random frequency hopping of which dwell time can be shorter than a chip. For the maximum frequency dwelling time (i.e., T_c) [21], the FHBOC modulated baseband signal is expressed as

$$y_{FH} = C(t) \sum_{k=0}^{N-1} p_{FH}\left(t - kT_c, f_{sc}^k\right), \tag{21}$$

where

$$p_{FH}\left(t, f_{sc}^k\right) = \begin{cases} \text{sign}\left(\sin\left(2\pi f_{sc}^k t\right)\right), & 0 \le t \le T_c \\ 0, & \text{otherwise} \end{cases}, \tag{22}$$

and $f_{sc}^k \left(f_l \le f_{sc}^k \le f_h\right)$ is the subcarrier frequency in the hopset for the k-th spreading code chip.

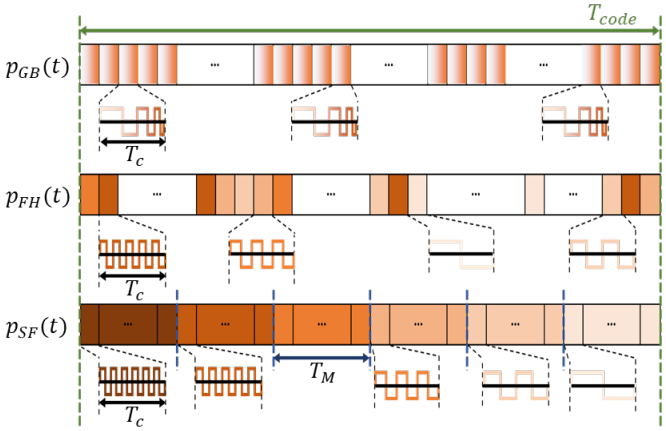

Fig. 6. Subcarrier waveforms for GBOC(6,1,0) $p_{GB}(t)$, FHBOC(6:1:1,1) $p_{FH}(t)$, and SFBOC(6:-1:1,1) $p_{SF}(t)$.

Fig. 6 compares subcarrier waveforms $P_{GB}(t)$, $P_{FH}(t)$, and $P_{SF}(t)$, where the height of the subcarrier frequency expressed with the darkness of the color in each modulation (i.e., darker color represents higher frequency). Note that GBOC has the instantaneous frequency dwelling time, and FHBOC has much shorter frequency dwelling time (T_c) than SFBOC. The correlation properties of the three modulations in Fig. 6 are compared in Appendix C.

B. Robustness to interference

In this subsection, we compare and analyze the intersystem interference of the proposed SFBOC and all compared modulations. A new GNSS signal is very likely to share the popular GNSS band currently in service [17], [20], [21]. Since the proposed SFBOC has a TVSF, it interferes with various signals within a wider band than the conventional (fixed subcarrier frequency) GNSS modulations. We show the PSDs for SFBOC(6:-1:1,1) and all compared modulations in Fig. 7.

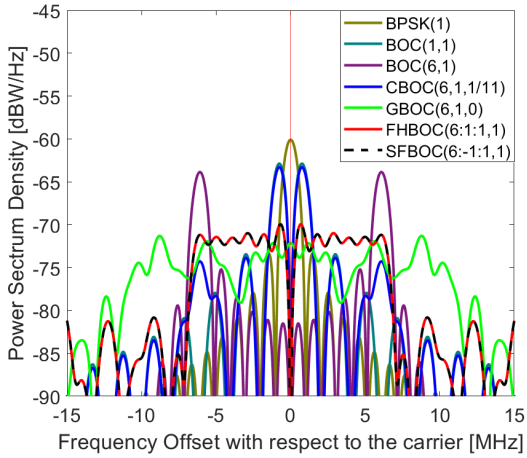

Fig. 7. PSDs for SFBOC(6:-1:1,1) and all compared modulations.

Fig. 7 shows the PSDs of SFBOC(6:-1:1,1) and all compared modulations. As shown, the null-to-null bandwidth of SFBOC(6:-1:1,1) and modulations with TVSF are (generally) much wider and the PSD magnitudes are much lower than the conventional GNSS modulations. Therefore, SFBOC(6:-1:1,1) and modulations with TVSF are expected to have smaller intersystem interference than conventional GNSS modulations. Note that in the case of GBOC(6,1,0), the PSD is widely spread but not uniform. The PSD of GBOC(6,1,0) has a null-to-null bandwidth of $24f_0$ (i.e., from $-12f_0$ to $12f_0$) that is wider than that of SFBOC(6:-1:1,1) and FHBOC(6:1:1,1) whose null-to-null bandwidth is $14f_0$.

For a numerical comparison of intersystem interference, we calculate the SSC [20] representing the spectral overlap between signals $G_i(f)$ and $G_d(f)$ as

$$SSC = \int_{-BW_d}^{BW_d} G_i(f) G_d(f) df, \tag{23}$$

where $G_i(f)$ is the PSD of the considered signal, $G_d(f)$ is the PSD of the counterpart signal.

As shown in Fig. 7, FHBOC(6:1:1,1) has the same PSD and $SSC(23)$ to SFBOC(6:-1:1,1). Note that GBOC(6,1,0) has a wider and lower PSD than SFBOC(6:-1:1,1) and FHBOC(6:1:1,1), resulting in about 2dB lower $SSC(23)$ on average, as shown in Table II. Since the $SSC(23)$ of the modulations with TVSF is significantly lower than that of the conventional GNSS modulations, the intersystem interference by the modulations with TVSF is much smaller than caused by the conventional GNSS signals. For example, BPSK(1) has the strongest intersystem interference. However, BOC(6,1) shows the lowest $SSC(23)$ in fact, because the PSD main lobe is well separated and located at around $\pm 6 \times f_0$.

TABLE II
SSC FOR SFBOC(6:-1:1,1) AND ALL COMPARED MODULATIONS.

SSC[dB]	BPSK(1)	BOC(1,1)	BOC(6,1)	CBOC(6,1,1/11)	GBOC(6,1,0)	SFBOC(6:-1:1,1), FHBOC(6:1:1,1)
BPSK(1)	-61.84	-67.84	-83.22	-68.24	-72.81	-73.86
BOC(1,1)	-67.84	-64.82	-83.20	-65.22	-73.27	-71.37
BOC(6,1)	-83.22	-83.20	-66.14	-75.78	-74.06	-72.64
CBOC(6,1,1/11)	-68.24	-65.22	-75.78	-65.60	-73.33	-71.47
GBOC(6,1,0)	-72.81	-73.27	-74.06	-73.33	-73.99	-74.44
SFBOC(6:-1:1,1), FHBOC(6:1:1,1)	-73.86	-71.37	-72.64	-71.47	-74.44	-72.16

TABLE III
PROCESSING GAINS FOR SFBOC(6:-1:1,1) AND ALL COMPARED MODULATIONS.

	BPSK(1)	BOC(1,1)	BOC(6,1)	CBOC(6,1,1/11)	SFBOC(6:-1:1,1), FHBOC(6:1:1,1)
P_G[dB]	43.11	46.11	46.11	43.10	53.89

Next, we analyze the anti-interference performance against narrowband interferences. In the spread spectrum systems, the processing gain P_G is determined by the spectral shape and is directly related to the anti-interference performance against narrowband signals. The processing gain of BPSK(n) $P_{G,BPSK}$ is found in [32] as

$$P_{G,BPSK} = \left[\frac{BW_{SS}}{BW_{DT}}\right]_{\text{dB}} = 10\log\left(n \times f_0/f_{DT}\right), \quad (24)$$

where BW_{ss}, BW_{DT} are spectrum bandwidth and the bandwidth required to send data, respectively, and f_{DT} is the data rate. Processing gain $P_{G,BOC}$ for BOC(m,n) [21], [32] signal is

$$P_{G,BOC} \cong 10\log\left(n \times \frac{f_0}{f_{DT}}\right) + 3, \quad (25)$$

and the processing gain $P_{G,SF}$ for SFBOC(m_h:$-i_m$:m_l,n) can be found in as

$$P_{G,SF} \cong 10\log\left(n \times \frac{f_0}{f_{DT}}\right) + 10\log\left(\frac{m_h - m_l}{n} + 1\right) + 3. \quad (26)$$

Therefore, $P_{G,BOC}$(25) is 3dB higher than $P_{G,BPSK}$(24) at the same code rate $f_c(= nf_0)$, $P_{G,SF}$ (26) is $10\log\left[\left(m_h - m_l\right)/n + 1\right]$ dB higher than $P_{G,BOC}$(25). This means that SFBOC is better in anti-narrowband interference than BOC of the same code rate. Table III shows the P_G of SFBOC(6:-1:1,1) and all compared modulations for the same data rate f_{DT}. For reference, GBOC is excluded from the table, because it is difficult to make a closed-form expression due to its unstructured spectrum shown in Fig. 7. However, as shown in Fig. 7, GBOC(6,1,0) has a wider PSD with lower magnitude than SFBOC(6:-1:1,1), so P_G of the GBOC is expected to be slightly better than that of modulations with TVSF.

In Table III, BOC(1,1) and BOC(6,1), which have a split spectrum of BPSK(1), have 3 dB higher P_G than BPSK(1) and have P_G similar to CBOC(6,1,1/11). P_G of SFBOC(6:-1:1,1) and FHBOC(6:1:1,1) is the highest in the table, because of the widest spectrum among all compared modulations except the GBOC(6,1,0). This result demonstrates that SFBOC(6:-1:1,1) and FHBOC(6:1:1,1) are very robust to the narrow band interference compared to conventional GNSS modulations.

The bandwidth efficiency of the spectrum is numerically compared through Fractional Out-of-Band Power (FOBP) analysis in Appendix D.

C. Ranging Accuracy

In this subsection, we compare the ranging accuracy of the proposed SFBOC and all compared modulations. When the delay estimation error variance $\text{var}\left(\hat{\tau}_0\right)$ is expressed in terms of the signal $y(t)$ with its bandwidth BW and a signal observation time (i.e., correlation length) T in additive white Gaussian noise (AWGN) channel with two-sided PSD of the noise $\text{N}_0/2$, it has been found [33], [34] that

$$\text{var}\left(\hat{\tau}_0\right) \geq \frac{\text{N}_0}{2\int_0^T \left(\frac{dy(t)}{dt}\right)^2 dt}, \quad (27)$$

where $\text{N}_0 = -204$ dBW/Hz. On the other hand, the Cramer-Rao Lower Bound(CRLB) of the delay estimation error is defined as

$$\text{var}\left(\hat{\tau}_0\right) = \text{N}_0/\left(2E_y\overline{F^2}\right), \quad (28)$$

where E_y is the signal energy. The mean square bandwidth (MSB) $\overline{F^2}$ is defined [33] as

$$\overline{F^2} = \int_{-BW_o}^{BW_o} \frac{(2\pi f)^2 |G_y(f)|^2 df}{|G_y(f)|^2 df}, \quad (29)$$

where $G_y(f)$ is the PSD of the signal $y(t)$. Therefore, smaller $\text{var}(\hat{\tau}_0)$ (27) is desirable with larger MSB $\overline{F^2}$ (29). On the other hand, since positioning performance depends on the sharpness of the main lobe peak of the bandlimited ACF output $\widetilde{R}_y(\tau)$ of $y(t)$, MSB $\overline{F^2}$ is defined in terms of $\widetilde{R}_s(\tau)$ [4], [20], [34] as

$$\overline{F^2} = \frac{-1}{\widetilde{R}_y(\tau)} \frac{d^2 \widetilde{R}_y(\tau)}{d\tau^2}\bigg|_{\tau=0} = \frac{4\pi^2}{\widetilde{R}_y(0)} \int_{-BW_o}^{BW_o} f^2 G_y(f) df. \quad (30)$$

Fig. 8 shows the Gabor bandwidth $\text{GB} = \sqrt{\overline{F^2}}/2\pi$ with respect to the single-sideband bandwidth BW_0 for all compared modulations and SFBOC(6:-1:1,1). As shown, all modulations converge to GB at around null-to-null bandwidth of the modulation; BPSK(1) and BOC(1,1) have GB less than 2MHz for almost all BW_o, and BOC(6,1), CBOC(6,1,1/11), SFBOC(6:-1:1,1), and FHBOC(6:1:1,1) converge to GB at around $BW_o = 7f_0$. However, as shown in Fig. 7, GBOC(6,1,0)

has a wider PSD than SFBOC(6:-1:1,1), and FHBOC(6:1:1,1) resulting in an increasing GB of GBOC(6,1,0) with the bandwidth BW_o. Note that among modulations of the same null-to-null bandwidth, CBOC(6,1,1/11) shows the lowest GB, since it has most of its spectrum concentrated at $|f| = f_0$ (similar to BOC(1,1)). On the other hand, since the PSD of BOC(6,1) has its spectrum concentrated at $|f| = 6f_0$, its GB becomes the largest at around $BW_o = 7f_0$. Note also that since FHBOC(6:1:1,1) and SFBOC(6:-1:1,1) have the same ACF output, SFBOC and FHBOC have the same PSD that is almost uniform in $|f| \leq 7f_0$, and their GB's are the same and almost linearly increasing up to $BW_o \leq 7f_0$. As expressed in

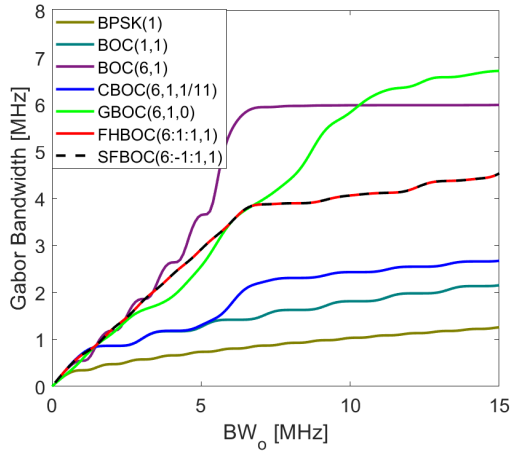

Fig. 8. Comparison of Gabor bandwidth for SFBOC(6:-1:1,1) and all compared modulations with respect to the single sideband bandwidth.

(30), ranging accuracy depends on the sharpness of the ACF output peak, the result shown in Fig. 8 is consistent with the sharpness of the ACF output peaks shown in Fig. 3a and Fig. 19 in Appendix B. That is, SFBOC(6:-1:1,1) has the same ranging accuracy to FHBOC(6:1:1,1), and the SFBOC and FHBOC have a slightly lower range accuracy compared to BOC(6,1) and GBOC(6,1,1/11).

D. Performance of the code discriminator

In this subsection, we investigate the S-curves of the modulations considered in this paper. S-curve is the response of the Early-Late (EL) discriminator [1], [14], [15] that is widely used in the tracking function of conventional GNSS receivers. We compare tracking errors of the Noncoherent Early-Late-Prompt (NELP) processing correlator [1] in AWGN channels.

Based on the ACF output $R(\epsilon)$ discussed in subsection II-B, the response of the EL discriminator is defined as

$$D(\epsilon) = R^2\left(\epsilon - \frac{\Delta}{2}\right) - R^2\left(\epsilon + \frac{\Delta}{2}\right), \tag{31}$$

where ϵ and Δ are the code phase tracking error and early-late spacing of the EL correlators, respectively. Fig. 9 shows the S-curve - EL discriminator output with respect to the normalized code tracking error ϵ/T_c of all compared modulations for $\Delta = 0.04T_c$. The ideal S-curve is characterized by a zero response outside the region of linearity (ROL) around $\epsilon = 0$. Within the ROL of the S-curve around $\epsilon = 0$, SFBOC(6:-1:1,1) and all compared modulations may have acceptable performance, however, the S-curves outside the ROL are very different. For example, SFBOC(6:-1:1,1) and modulations with TVSF have good correlation properties (see Appendix B), which results in excellent S-curves.

That means, SFBOC(6:-1:1,1) and modulations with TVSF have larger $D(\epsilon)$ (31) within ROL and smaller $D(\epsilon)$ outside the ROL than the conventional GNSS modulations. On the contrary, BPSK(1), BOC(1,1), and CBOC(6,1,1/11) show a low slope within ROL as shown in Fig. 9. In addition, BOC(6,1) has large side peaks that can cause unstable tracking performance. Note that steeper slope in the ROL and smaller side peaks in the S-curve lead to lower tracking ambiguity and better tracking performance [1] of the conventional EL discriminator-based tracking function. From this viewpoint, the SFBOC(6:-1:1,1) and modulations with TVSF in Fig. 9 show S-curves closer to ideal [1] than the conventional GNSS modulations. Therefore, SFBOC(6:-1:1,1) and modulations with TVSF are expected to have more robust positioning performance than conventional GNSS modulations in multipath and noisy channels. In Appendix C, the slopes within the ROL for various Δ's are compared.

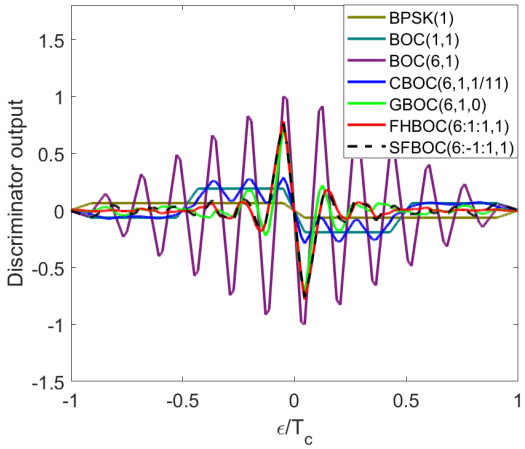

Fig. 9. Early-Late Discriminator output for SFBOC(6:-1:1,1) and all compared modulations with $\Delta = 0.04T_c$.

In [1], code tracking error variance σ^2_{NELP} for a delay-lock loop with NELP is found for AWGN channels as

$$\sigma^2_{NELP} = \zeta \frac{J_0\left(\frac{C}{N_0}\right)^{-1}}{J_2^2}\left[1 + \frac{1}{T_{corr}}\frac{J_1\left(\frac{C}{N_0}\right)^{-1}}{J_3^2}\right], \tag{32}$$

where

$$\zeta = \frac{c^2 BW_o\left(1 - 0.5BW_o T_{corr}\right)}{(2\pi)^2}, \tag{33}$$

$$\begin{bmatrix} J_0 \\ J_1 \end{bmatrix} = \int_{-BW_o}^{BW_o} G(f) \begin{bmatrix} \sin^2(\pi f\Delta) \\ \cos^2(\pi f\Delta) \end{bmatrix} df, \tag{34}$$

$$J_2 = \int_{-BW_o}^{BW_o} fG(f)\sin(\pi f\Delta)\,df, \tag{35}$$

$$J_3 = \int_{-BW_o}^{BW_o} G(f)\cos(\pi f\Delta)\,df, \tag{36}$$

c is the speed of light, T_{corr} is the correlation length, and $\mathrm{C/N_0}$ and BW_0 are the carrier power to noise spectral density ratio and the single-sideband bandwidth, respectively. The terms in the square brackets in (32) represent the squaring loss for non-coherent processing. When $\mathrm{C/N_0}$ is large, the squaring loss term becomes negligible, and the NELP error variance (32) is simplified to [20]

$$\sigma^2_{NELP} = \zeta J_0 \frac{\left(\frac{\mathrm{C}}{\mathrm{N_0}}\right)^{-1}}{J_2^2} = \Psi \times BW_o\left(1 - 0.5BW_oT\right)\left(\frac{\mathrm{C}}{\mathrm{N_0}}\right)^{-1}, \tag{37}$$

where $\Psi \equiv c^2J_0/\left(2\pi J_2\right)^2$. As a result, σ^2_{NELP} can be evaluated in terms of Ψ with respect to BW_o for a given $\mathrm{C/N_0}$ and T. Fig. 10 shows the comparative performance Ψ with respect to the BW_0 for SFBOC(6:-1:1,1) and all compared modulations for $\Delta = 0.04T_c$. As shown in Fig. 10,

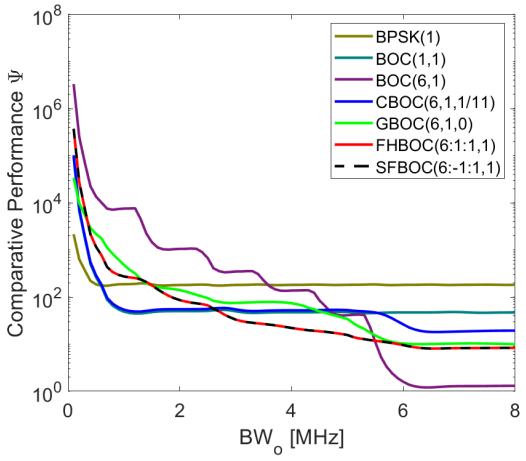

Fig. 10. Comparative Performance Ψ of SFBOC(6:-1:1,1) and all compared modulations.

Ψ decreases as BW_o increases for all modulations, contrary to the Gabor bandwidth in subsection III-C. As shown, BOC(6,1) has the highest and lowest Ψ for $BW_o < 4$MHz and about $BW_o > 5.5$MHz, respectively. That is BOC(6,1) achieves the highest accuracy when BW_o is large enough, since its spectrum is concentrated around $BW_o = \pm 6$MHz. GBOC(6,1,0) has slightly higher or almost the same Ψ to SFBOC(6:-1:1,1) and FHBOC(6:1:1,1). This is different from the trend of GB with respect to the bandwidth, shown in Fig. 8. As a summary, it is found that while SFBOC(6:-1:1,1) has superior tracking performance than BPSK(1), BOC(1,1), and CBOC(6,1,1/11) and similar tracking performance to other modulations with TVSF, it has inferior tracking performance to BOC(6,1) for $BW_o > 5.5f_0$.

E. Multipath mitigation

Multipath interference is one of the major error sources in GNSS systems. In this subsection, we compare the Multipath Error Envelope (MEE) [31] of SFBOC and all compared modulations. Fig. 11a shows MEE for a two-path channel, when pre-correlation bandwidth $PCBW = 20$MHz and early-late correlator chip spacing $\Delta = 0.1T_c$, and second path delay τ is uniform in $[0, 1.5T_c]$. Fig. 11b shows average ranging error for the MEE shown in Fig. 11a. The mathematical expression to generate the MEE shown in Fig. 11 is found in [31] as

$$\left[R\left(\epsilon-\frac{\Delta}{2}\right)\pm\alpha R\left(\epsilon-\tau-\frac{\Delta}{2}\right)\right]^2 - \left[R\left(\epsilon+\frac{\Delta}{2}\right)\pm\alpha R\left(\epsilon-\tau+\frac{\Delta}{2}\right)\right]^2 = 0, \tag{38}$$

where $\alpha(=0.5)$ is the magnitude ratio of the second path to the first path (i.e., LOS signal). Since SFBOC(6:-1:1,1) and modulations with TVSF (i.e., GBOC(6,1,0) and FHBOC(6:1:1,1)) have similar ACF outputs as shown in Fig. 19 in Appendix B, SFBOC(6:-1:1,1) shows similar performance to modulations with TVSF as shown in Fig. 11a. When compared to BOC(6,1), SFBOC(6:-1:1,1) shows slightly larger range error at $\tau < 40$m due to the slightly wider ACF output main lobe, but shows much smaller range error at $\tau \geq 40$m due to the much smaller side peaks of the ACF output. In addition, as τ increases, the average ranging error of SFBOC(6:-1:1,1) shown in Fig. 11b becomes much smaller than those of the conventional GNSS modulations and decreases rapidly. These results show that multipath mitigation performance of the proposed SFBOC is similar to modulations with TVSF and is better than the conventional GNSS modulations.

F. Code-Doppler effect

Due to the Doppler frequency in the incoming signal, companding occurs in the baseband square waveform (in other words, code-Doppler) of the received GNSS signals, which results in a reduced ACF output peak (in other words, loss of signal energy). Let the received signal with the code-Doppler be $y'(t)(=y(t(1-\lambda)))$, where $\lambda = (dr/dt)/c$, r is the distance between the satellite and the receiver, and $y(t)$ is the intact signal without the code-Doppler. And let the carrier frequency f'_r of the received signal with Doppler be

$$f'_r = f_r + f_{Dopp}, \tag{39}$$

where f_{Dopp} is Doppler frequency to the carrier and $f_{Dopp} = -\lambda f_r$. According to [35], GPS L1 band C/A code signal receiver has the maximum code-Doppler frequency can be ± 6.5Hz. Then, the code-Doppler frequency f_{cd} of $y'(t)$ can be found as

$$f_{cd} = f_c \times \lambda = f_c \times \frac{f_{Dopp}}{f_r}, \tag{40}$$

and the normalized cross-correlation output between $y'(t)$ and the receiver replica signal $s(t)$ can be expressed as

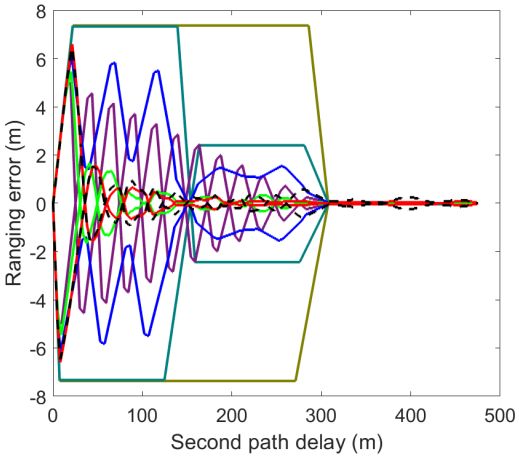

(a) Multipath Error Envelopes

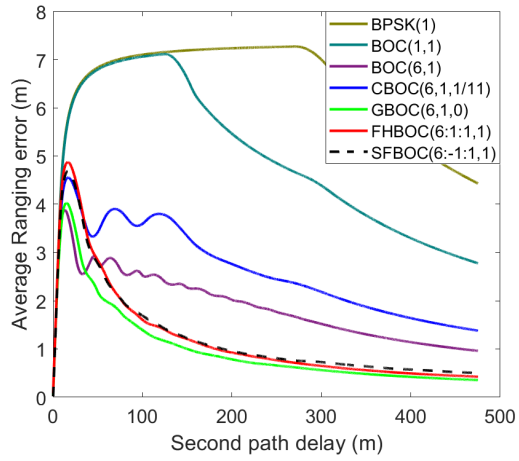

(b) Average Multipath Error

Fig. 11. Tracking error comparison in a two-path channel for all compared modulations.

$$R_{sy'}(\tau \mid \lambda) = \frac{1}{T_{corr}} \int_0^{T_{corr}} s(t)\,(y'(t-\tau))^*\,dt,$$
$$= \frac{1}{T_{corr}} \int_0^{T_{corr}} s(t)(y(t(1-\lambda)-\tau))^* dt. \quad (41)$$

We compare the peak value of $R_{sy'}(\tau \mid \lambda)$(41) for BPSK(1), BOC(6,1), SFBOC(6:-1:1,1) and modulations with TVSF (i.e., FHBOC(6:1:1,1) and GBOC(6,1,0)) as shown in Fig. 12. Since the effect of square waveform companding due to f_{cd} (40) on $R_{sy'}(\tau \mid \lambda)$(41) deteriorate with the correlation length T_{corr} and the random sampling time offset (STO), we consider various $T_{corr} = 1, 2, 5$, and 10 [ms] and random STO within sampling interval $[0, T_s]$ in Fig. 12. That means, we show the average of ACF output peak values for 100 random STOs.

In Fig. 12a, Fig. 12b, and Fig. 12c, we show simulation results for $f_s = 120f_0$, $f_s = 24f_0$, and $f_s = 12f_0$, respectively, where $f_s = 1/T_s$ is the sampling frequency. Note that $f_s = 120f_0$ allows even sampling of all subcarriers with different frequency constituting SFBOC((6:-1:1,1) and FHBOC(6:1:1,1), $f_s = 24f_0$ does not allow even sampling of BOC(5,1), and $f_s = 12f_0$ does not allow even sampling of BOC(4,1) and BOC(5,1). For example, there are five subcarrier periods per T_c in BOC(5,1), and $f_s = 24f_0$ generates twenty-four samples per a chip. Consequently, there are 4.8 samples per a (sine-based) subcarrier, which means there are $2 \sim 3$ positive valued samples from the first half of the sine function and $2 \sim 3$ negative valued samples from the last half, depending on the sampling offset which is assumed random and unknown. This happens to both the received signal and the receiver replica signal $s(t)$ in 41, so that $s(t)$ may have different number of positive and negative samples from those of the received signal. As a result, there can be a significant degradation in the peak value of the ACF output.

Overall, Fig. 12a shows better results than Fig. 12b and Fig. 12c, because there is no uneven sampling of BOC signals with different subcarrier frequencies. BPSK(1) maintains 0.98 or higher peak value for all code-Doppler range, because an ideal BPSK(1) square waveform has the same magnitude over the entire chip interval so that any STO would result in all $+1$ samples. On the other hand, GBOC(6,1,0) shows the worst performance so that it is the most vulnerable modulation among all compared modulations. As shown at $f_{cd} = 0$ in all of the three figures, GBOC(6,1) suffers from the decrease of the sampling rate from $f_s = 120f_0$ to $f_s = 12f_0$, and reveals considerable peak value degradation in the ACF output for the increase of $|f_c d|$ and T_{corr}. In the three figures, BOC(6,1) is slightly better than GBOC(6,1), but it shows the largest peak value (of the ACF output) change among all compared modulations. In other words, the difference between the decrease of the peak values of BOC(6,1) for $T_{corr} = 1$ms and $T_{corr} = 10$ms is largest (e.g., more than 0.35) at $f_{cd} = 6.5$Hz as shown in all figures. Therefore, BPSK(1) is the most robust and GBOC(6,1) and BOC(6,1) are very vulnerable to the code-Doppler and STO among all compared modulations.

In the case of SFBOC(6:-1:1,1) and FHBOC(6:1:1,1), the performance shown in the three figures of Fig. 12 is the same. Their performance degrades with the decrease of the sampling frequency, which may be similar to GBOC(6,1), however, the performance degradation is much smaller than GBOC(6,1) as shown in Fig. 12c. And the change in the peak values (of the ACF output) of SFBOC(6:-1:1,1) and FHBOC(6:1:1,1) are similar to that of GBOC(6,1) but much smaller than BOC(6,1) as shown in the three figures. However, for small $|f_{cd}|$, the peak values of SFBOC(6:-1:1,1) and FHBOC(6:1:1,1) are smaller than the peak value of BOC(6,1), which is clearly shown in Fig. 12c. As a result, the proposed SFBOC and FHBOC have the same robustness to the code-Doppler and STO, which is superior than GBOC for all f_{cd} and T_{corr} but inferior than BPSK. And when compared to the BOC(6,1), SFBOC(6:-1:1,1) and FHBOC(6:1:1,1) are more robust when f_{cd} and T_{corr} are large.

G. Receiver complexity

In this subsection, we compare SFBOC and modulations with TVSF in the view of implementation complexity.

First, GBOC has a much wider spectrum than SFBOC (and FHBOC). The null-to-null bandwidth of GBOC(p,1,0)

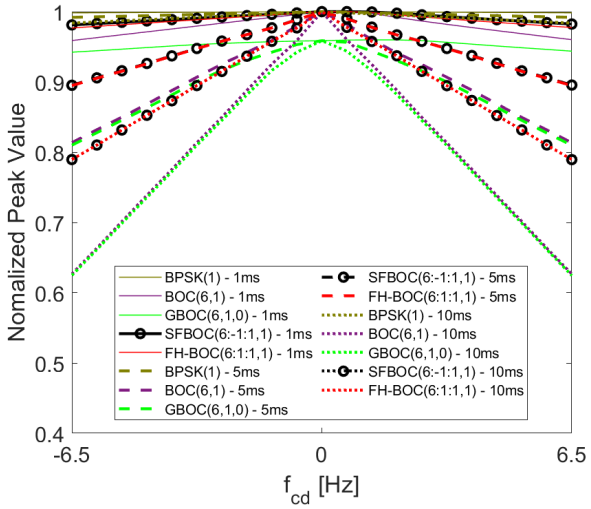

(a) $f_s = 120f_0$

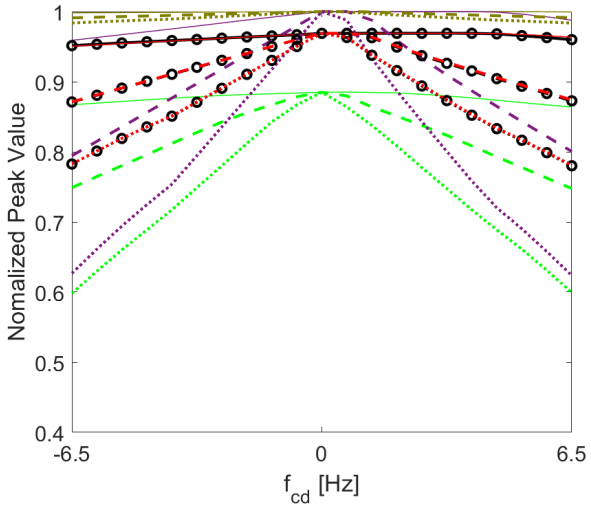

(b) $f_s = 24f_0$

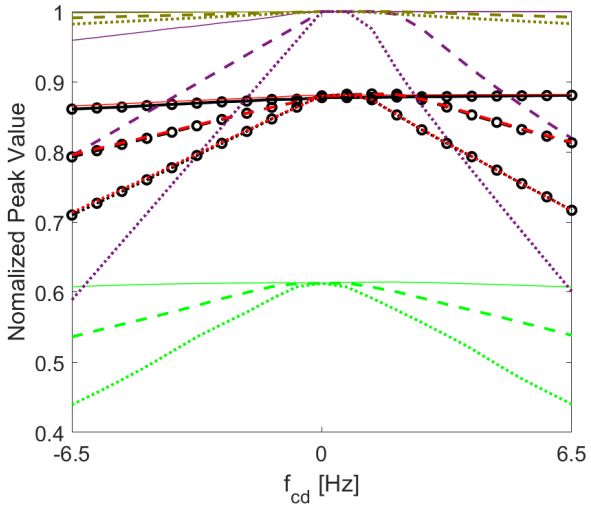

(c) $f_s = 12f_0$

Fig. 12. Loss of correlation for SFBOC and modulations with TVSF averaged over random STO.

and SFBOC(p:-1:1,1) for various p (i.e., $p = \{3, 4, \ldots 30\}$) is shown in Fig. 13. As shown, the difference between the null-to-null bandwidth of the two modulations (GBOC and SFBOC) increases almost linearly as p increases, and, on average, GBOC has about 1.8 times larger null-to-null bandwidth than that of SFBOC. Considering BOC(p,1) has the same null-to-null bandwidth to SFBOC(p:-1:1,1) as discussed in subsection II-C, we can conclude that a GBOC receiver requires much wider pre-correlation bandwidth (PCBW) than SFBOC and BOC receivers. Therefore, GBOC receiver may suffer from noise due to the wide PCBW and requires higher sampling frequency and more computational resource in the receiver.

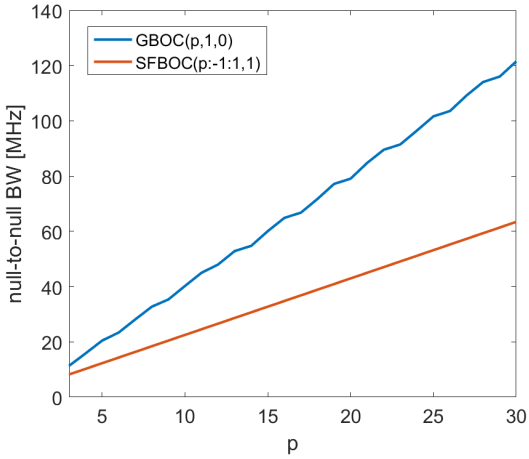

Fig. 13. Comparison of null-to-null bandwidth of GBOC and SFBOC.

Second, FHBOC receivers need additional hopping sequence search in the acquisition process [21], in addition to the code phase and Doppler frequency searches. The search space for FHBOC acquisition is found

$$N_{acq_{FH}} = N_f N_t N_p, \tag{42}$$

where N_f and N_t are the number of hypothesis to test in the Doppler frequency and code phase domains, respectively, and N_p is the ratio of the length of the frequency-hopping sequence to the spreading code sequence [21]. Therefore, considering the BOC acquisition that has a search space of size

$$N_{acq_{BOC}} = N_f N_t, \tag{43}$$

BOC acquisition has N_p times smaller search space than FHBOC acquisition. However, since SFBOC has a fixed subcarrier frequency during T_M, and the subcarrier frequency is deterministic over the entire T_{code}, SFBOC has the same search space to the BOC receiver. Note that when $N_p = 1$, FHBOC has the same search space to BOC and SFBOC, however, for a pseudorandom frequency-hopping sequence with a large $N_p (\gg 1)$ suggested by [21], there can be a noticeable disadvantage due to the large acquisition complexity.

IV. Single-Sideband Processing-Based Filterbank

For modulations with discrete TVSF such as proposed SFBOC and FHBOC, the frequency bandwidth occupied by the instantaneous BOC signal is very small when compared to

the entire frequency band. In addition, the difference between the instant and entire frequency bands continues to increase as the entire frequency band becomes wider. In this perspective, utilizing the relatively small frequency band occupied by the instantaneous BOC signal rather than the wide entire frequency band for the pre-correlation bandwidth [35] becomes necessary to improve SNR in the receiver. To this end, we introduce filterbank to process signals with discrete time-varying BOC subcarrier frequency (i.e., SFBOC and FHBOC), and we show that FHBOC reveals a severe blanking problem that there can be a significant loss of the first arrival path when a later arrival path is a dominant path in the received signal.

A. SBPFB Structure

As shown in Fig. 14, Single-sideband Processing-based Filterbank (SBPFB) is a mere combination of the single-sideband processing (SBP) [25] and a filterbank [36], which can be used when the approximate code phase of the received signal is detected by the acquisition process. SBP has Upper and Lower sideband filters, so that the SBP separates duel-sideband spectrum of BOC signals into upper (red dotted line block) and lower (blue dotted line block) single sideband spectrums. In the end, SBP combines the separately processed signals non-coherently [25] as shown in Fig. 14. For convenience of explanation, we assume ideal sideband filters in the SBPFB, and $H_u(f)$ and $H_l(f)$ can be defined as follows

$$H_u(f) = \begin{cases} 1, & f_{IF} \le f \le f_{IF} + BW_D/2 \\ 0, & \text{otherwise} \end{cases}, \tag{44}$$

$$H_l(f) = \begin{cases} 1, & -BW_D/2 + f_{IF} \le f \le f_{IF} \\ 0, & \text{otherwise} \end{cases}, \tag{45}$$

where BW_D is the overall bandwidth (dual-sideband) of the signal. Considering the PCBW $BW_D \ge 2(m_h f_0 + f_c)$ as suggested in [35], we assume that $BW_D = 2(m_h f_0 + 2f_c)$. Note also that since $H_u(f)$ (44) and $H_l(f)$ (45) differ only in the filter band, we only describe upper sideband processing in the following. As shown, the filterbank has N_M parallel band-pass filters (BPF): $H_1(f), H_2(f),\ldots$, and $H_{N_{M-1}}(f)$, where an ideal BPF $H_k(f)$ of the filterbank can be defined as

$$H_k(f) = \begin{cases} 1, & |f - m_k f_0| \le BW_h/2 \\ 0, & \text{otherwise} \end{cases}, \tag{46}$$

where $k = \{0, 1, \ldots N_M - 1\}$, and BW_h is larger than the minimum $2f_c$, such that $2f_c \le BW_h \ll BW_D/2$, to process the instantaneous BOC($m_k, 1$) signal with a center frequency $m_k\ f_0$) that constitutes SFBOC or FHBOC. Note that, when the filterbank is applied to the FHBOC signal, the number of parallel BPFs should be equal to the number of distinctive hopping frequencies in the hopset (21). However, for the simplicity of explanation, we assume the case when the filterbank is applied to the SFBOC in the following.

The SFBOC signal at the intermediate frequency (IF) $y_{IF}(t)$ can be written as

$$\begin{aligned} y_{IF}(t) = {} & C\left(t-\tau_r\right) p_{SF}\left(t-\tau_r\right) \\ & \times \exp\left[j2\pi\left(f_{IF}+f_d\right)\left(t-\tau_r\right)+\varphi_r\right] + v(t), \end{aligned} \tag{47}$$

where $p_{SF}(t) = \text{sign}\left[\sin\left(2\pi M_k(t) f_0(t)\right)\right]$ (11), and τ_r, f_d, φ_r, and $v(t)$ are the code phase, Doppler frequency, unknown carrier phase of received signal, and a zero-mean AWGN process with two-sided PSD $\mathrm{N}_0/2$, respectively. Then, the upper sideband filter output $y^+_{IF}(t)$ is

$$y^+_{IF}(t) = y_{IF}(t) * h_u(t), \tag{48}$$

where $h_u(t) = \mathcal{F}^{-1}\left\{H_u(f)\right\}$ represents the Inverse Fourier Transform of $H_u(f)$, and $(\cdot)^+$ indicates the upper sideband. The noise output $v^+(t)$ of the upper sideband filter is a zero-mean AWGN process with a variance of $BW_D\mathrm{N}_0/2$. Passing $y^+_{IF}(t)$ through the k-th BPF $H_k(f)$ of the filterbank yields

$$\begin{aligned} \widetilde{y}^+_{IF_k}(t) &= y^+_{IF}(t) * h_k(t) \\ &\cong C(t-\tau_r)\exp\left[j2\pi(f_{IF}+m_k f_0+f_d)\right. \\ &\qquad \left.\times(t-\tau_r)+\varphi'_r\right] + \widetilde{v}^+(t), \end{aligned} \tag{49}$$

where $h_k(t) = \mathcal{F}^{-1}\{H_k(f)\}$ and φ'_r is an unknown carrier phase. Since $\widetilde{v}^+(t)$ is the band-limited $v(t)$ over the BPF bandwidth BW_h, the power of $\widetilde{v}^+(t)$ is reduced by BW_D/BW_h times compared to the power of $v^+(t)$. Notice that $\widetilde{y}^+_{IF_k}(t)$ has a similar PSD to a BPSK signal with a center frequency $f_r = f_{IF} + m_k f_0$. The Output Switch block selects the output of the appropriate BPF among the N_M BPF outputs; we assume that k-th BPF $H_k(f)$ (46) that produces $\widetilde{y}^+_{IF_k}(t)$ whose instantaneous subcarrier frequency is $m_k f_0$ during the frequency dwelling time T_M (10). The baseband signal can be found after a frequency down-conversion and an ideal low pass filtering as

$$\begin{aligned} \widetilde{y}^+_{BB}(t) &= \left(\widetilde{y}^+_{IF}(t)\cos\left(2\pi f_{IF}t\right)\right) * h_{LPF}(t) \\ &= C(t-\tau_r)\exp\left[j2\pi(m_k f_0+f_d)\right. \\ &\qquad \left.\times(t-\tau_r)+\varphi''_r\right] + \widetilde{n}^+(t), \end{aligned} \tag{50}$$

where

$$h_{LPF}(t) = \mathcal{F}^{-1}\left\{H_{LPF}(f)\right\}, \tag{51}$$

$$H_{LPF}(f) = \begin{cases} 1, 0 \le f \le BW_D/2 \\ 0, \text{otherwise} \end{cases}, \tag{52}$$

where φ''_r is the unknown carrier phase, $\widetilde{n}^+(t)$ is a zero-mean AWGN process with variance $BW_h N_0/2$. A baseband replica of the single-sideband

$$\begin{aligned} s_{BB}(t) = {} & C\left(t-\tau_r\right) \\ & \times \sum_{k=0}^{N_M-1} \text{sign}\left[\sin\left(2\pi M_k\left(t-\tau_r\right) f_0\left(t-\tau_r\right)\right)\right] \end{aligned} \tag{53}$$

is generated and converted to $s^+_{BB}(t)$ through the upper sideband filter as shown in Fig. 14 and then correlated with $\widetilde{y}^+_{BB}(t)$ (50) in the tracking loop. The correlation result of $s^+_{BB}(t)$ and $\widetilde{y}^+_{BB}(t)$ (50) is non-coherently combined with the final output of the lower sideband processing. Note that SBPFB can be applied to FHBOC with the Output Switch block selects BPF output corresponding to the correct subcarrier frequency that is hopping at every T_c. However, since GBOC has the subcarrier frequency continuously changing within T_c, SBPFB may need a large number of parallel PBKs and the Output Switch block should switch filter output selection instantaneously.

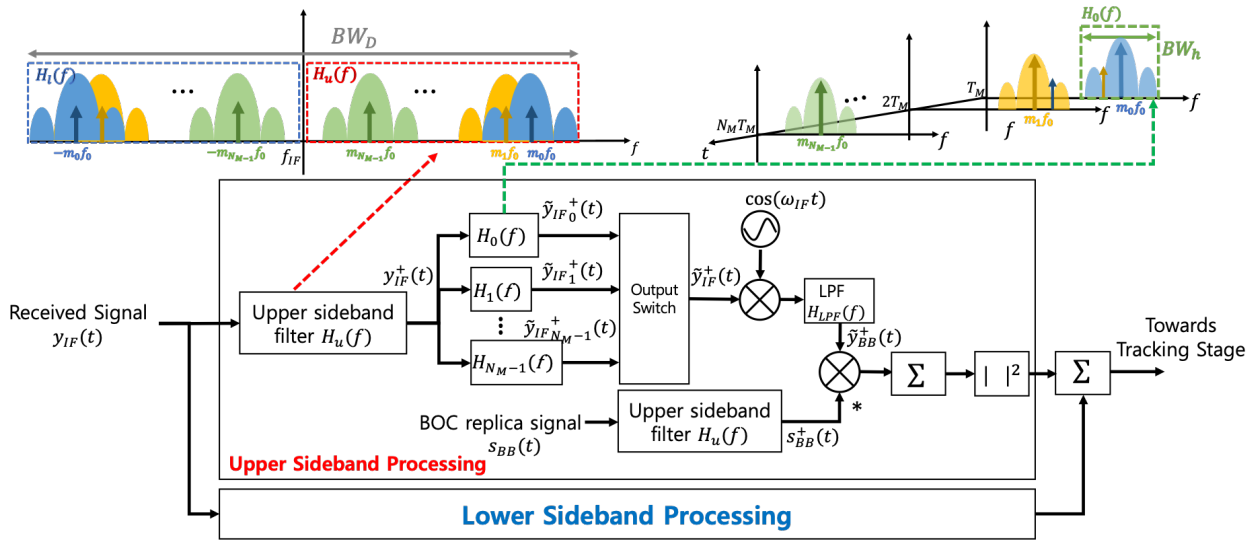

Fig. 14. Single-sideband processing-based Filterbank block diagram.

Compared to the dual-sideband processing (DBP), SBPFB receiver can have an SNR improvement by

$$\frac{\mathrm{SNR_{SBPFB}}}{\mathrm{SNR_{DBP}}} = \left[\frac{\frac{P_{y^+}}{BW_h \mathrm{N}_0}}{\frac{P_y}{BW_D \mathrm{N}_0}}\right]_{\mathrm{dB}} = \left[\frac{BW_D}{2BW_h}\right]_{\mathrm{dB}} = 10\log_{10}\left(\frac{m_h f_0/f_c + 1}{2}\right), \quad (54)$$

where $\mathrm{SNR_{DBP}}$ and $\mathrm{SNR_{SBPFB}}$ are the SNR of the DBP and SBPFB outputs, respectively, and P_y and P_y^+ indicate dual-sideband and single-sideband power of the received signal, respectively. Note that due to the SBPFB, the signal power is reduced by 3dB compared to the DBP (i.e., $P_{y^+} = P_y/2$). However, since the bandwidth of the BPF, BW_h ($BW_h > 2f_c$), of the filterbank is much smaller than that of the DBP receiver BW_D ($= 2(m_h f_0 + 4f_c)$, the SNR is greatly improved. For example, for SFBOC(10:-1:1,1), when we compare DBP with $BW_D = 24f_0$ to SBPFB with $BW_h = 4f_0$, we can expect about 7.8dB of SNR improvement. In the following, we compare the reference SNR $\mathrm{SNR_{ref}}$ [35] of a GNSS signal being received for a given PCBW and $\mathrm{C/N_0}$ to the post-correlation SNR $\mathrm{SNR_{post}}$ [37] at the ACF output, where $\mathrm{SNR_{ref}}$ and $\mathrm{SNR_{post}}$ are defined as

$$\mathrm{SNR_{ref}} = \frac{\mathrm{C}}{\mathrm{N_0} \times PCBW}, \quad (55)$$

$$\mathrm{SNR_{post}} = \frac{|R(0)|^2}{\mathrm{var}(\tilde{n}(t))^2}, \quad (56)$$

respectively, where $R(0)$ is the peak magnitude of the ACF output, and $\tilde{n}(t)$ indicates the noise level outside the main lobe of the ACF output. When $\mathrm{C/N_0}$ values in the receiver with PCBW $24f_0$ is ranging from 37 to 45 dBHz for useful signals [38], $\mathrm{SNR_{ref}}$ (55) becomes from -36.9 to -29.4 dB. Fig. 15 shows $\mathrm{SNR_{ref}}$ (55) and $\mathrm{SNR_{post}}$ (56) calculated using 100 Monte Carlo simulations for receivers using DBP and SBPFB, with respect to $\mathrm{C/N_0}$. As shown, the $\mathrm{SNR_{post}}$ for DBP (i.e., $\mathrm{SNR_{DBP}}$) is similar to $\mathrm{SNR_{ref}}$, since there is no special SNR improvement scheme applied, however, the $\mathrm{SNR_{post}}$ for SBPFB is improved by about 7∼8 dB from $\mathrm{SNR_{ref}}$, as expected.

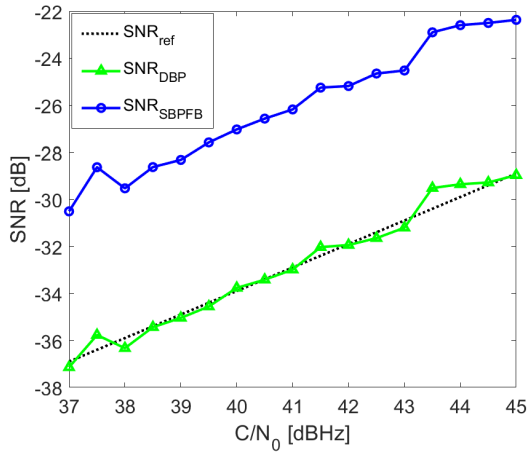

Fig. 15. SNR comparison between DBP and SBPFB for SFBOC(10:-1:1,1).

B. First Arrival Path Blanking in NLOS Multipath Channel

A receiver with SBPFB may process SFBOC and FHBOC, where the actual frequency of $\tilde{y}^+_{IF_k}(t)$ (49) varies at every frequency dwelling time of the signal. For FHBOC, whose subcarrier frequency varies at every T_c, the receiver with SBPFB should change the selection of BPF output (from the filterbank) at every T_c accordingly. However, in the NLOS multipath channel, where the first arrival path (FP) is not the dominant path, applying the BPF of the filterbank strictly limits the filter output to within the interval T_c, which results in a considerable loss of signal power of the FP. Let the signal $y_M(t)$ be the received signal from the NLOS multipath

channel environment as

$$y_M(t) = \sum_{j=0}^{N_{path}-1} \alpha_j y\left(t-\tau_j\right), \tag{57}$$

where α_j and τ_j denote unknown complex channel coefficients and unknown arrival time delays of the j-th path, respectively, and N_{path} denotes the number of paths in the received signal. For simplicity of explanation, we assume that $N_{path} = 2$ and $\alpha_0 < \alpha_1$. Fig. 16a and Fig. 16b show the simplified waveforms of the received signal modulated with FHBOC(6:1:1,1) and SFBOC(6:-1:1,1), respectively, in a NLOS two-path channel environment. We assume that the path delays τ_0 and τ_1 of FP (orange solid line) and the second path (SP, blue dashed line) are 0 and $0.5T_c$, respectively, and that $\alpha_0 = 1/2\alpha_1$. Since SP is the dominant path, Fig. 16 shows a simple case, where the signal code phase detected by the acquisition process is synchronized with the timing of the SP. The red dashed line in Fig. 16 indicates the temporal boundaries of the output of the BPF $H_k(f)$(46) selected by the Output Switch block. That is, the time interval selected by the Output Switch block exactly coincides with the chip boundary of the SP. In Fig. 16a, the sequence of the subcarrier frequency of the FHBOC (6:1:1,1) signal is $6f_0, 2f_0, 5f_0, f_0$ each with T_c interval within the overall depicted interval $3.5T_c$. In contrast, Fig. 16b shows the subcarrier frequency of the SFBOC(6:-1:1,1) signal changes from $6f_0$ to $5f_0$ within the same overall interval. As shown, when the FP is arriving at $0.5T_c$ earlier than SP, and the previous BPF and the current BPF $H_k(f)$ are not the same, half of the FP signal is blanked (i.e., not delivered) by the BPF operating at the SP chip boundary. As a result, the FHBOC(6:1:1,1) signal and SFBOC(6:-1:1,1) signal shown in Fig. 16 have FP signal blanked for total duration of $2T_c$ and $0.5T_c$, respectively, within the overall interval $3.5T_c$. If this situation continues to the whole code sequence T_{code}, FP blanking occurs for a total duration of $0.5N_M\ T_c$ for SFBOC(6:-1:1,1), but a severe FP blanking occurs for a total duration of (up to) $0.5T_{code}$ for FHBOC(6:-1:1). Note that the maximum $0.5T_{code}$ long FP blanking occurs when there is no subsequent subcarrier frequency same to the previous subcarrier frequency during T_{code} in the FHBOC.

Consequently, when severe FP blanking occurs, the peak magnitude of the FP signal is greatly attenuated at the correlation output (of $\widetilde{y}^{+}_{BB}(t)$ (50) and $s^{+}_{BB}(t)$), and tracking the FP in the tracking function becomes more difficult. However, for SFBOC(6:-1:1,1), severe FP blanking does not occur as there is no frequent subcarrier frequency change during a long frequency dwelling time(T_M), so the probability of losing the FP signal by the SBPFB is negligible. Therefore, SFBOC hardly loses FP signal while greatly improving SNR by SBPFB, but FHBOC has a large possibility of losing FP signal in the NLOS multipath environments. To numerically analyze the FP loss, we evaluate FHBOC(p:1:1,1) and SFBOC(p:-1:1,1) with $p = \{4, 6, 8\}$ for a two-path NLOS channel, and the result is shown in Fig. 17, where we evaluate the power ratio of FP and SP P_{FP}/P_{SP} at the SBPFB output. To prevent ACF output distortion [39] caused by pre-correlation bandwith (PCBW) [35] in the simulations, we assume that the BPF of

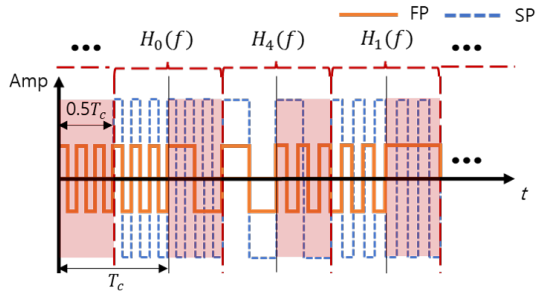

(a) FHBOC(6:1:1,1)

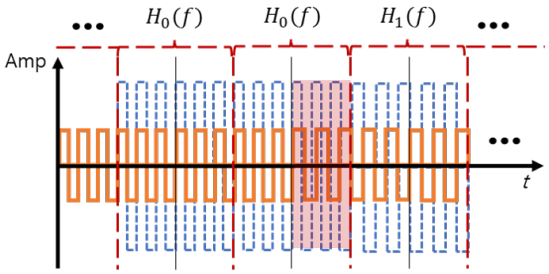

(b) SFBOC(6:-1:1,1)

Fig. 16. Example of received signals in NLOS two-path channel.

the filterbank has a wide BW such that $BW_h \geq 4f_c$. In Fig.

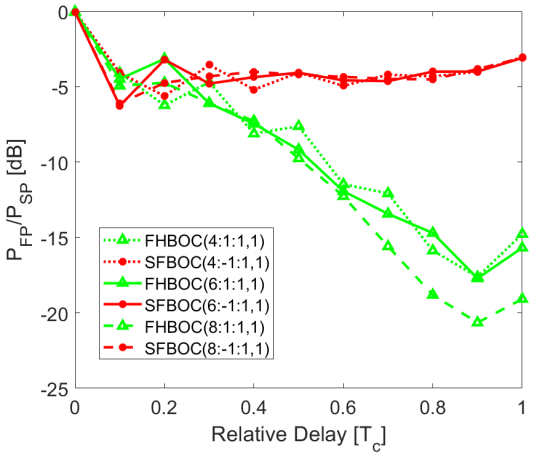

Fig. 17. ACF output power ratio of FP to SP for $\alpha_0 = \frac{1}{\sqrt{2}}\alpha_1$, and various relative delay $(\tau_1 - \tau_0)$.

17, we assume that $\alpha_0 = \frac{1}{\sqrt{2}}\alpha_1$ and the relative path delay $\tau_1 - \tau_0$ varies to show ACF output power ratio between the two paths P_{FP}/P_{SP}, where P_{signal} is the power of the signal at the ACF output. SFBOC shows P_{FP}/P_{SP} of about -3dB for all p and all relative delays, as expected. On the contrary, for FHBOC, P_{FP}/P_{SP} continues to decrease as the relative delay $\Delta\tau(= \tau_1 - \tau_0)$ increases, and P_{FP}/P_{SP} becomes lower for large p as the probability to have the same subsequent subcarrier frequency becomes smaller. Therefore, the loss of FP (i.e., blanking FP) can be severe and considerable for FHBOC. As a result, when FHBOC uses SBPFB in the NLOS multipath environments, FP tracking performance can be significantly

degraded and the resulting positioning performance can be poor.

V. Conclusion

In this study, we have proposed SFBOC modulation based on BOC and SFCW for a possible advanced GNSS signal of Korea Positioning System (KPS). In the SFBOC, BOC subcarrier frequency slowly decreases stepwise during the code period. In order to demonstrate the superiority of the proposed SFBOC, we have analyzed and compared the performance of SFBOC with those of all compared modulations in various aspects related to positioning performance. As a result, it has been demonstrated that the proposed SFBOC has superior correlation properties, excellent multipath and noise mitigation performance, and lower intersystem interference than the conventional GNSS modulations. When compared to the modulations with TVSF, we have shown that SFBOC is more robust to Doppler effects than GBOC, and has the advantage of shorter search time than FHBOC. In addition, we introduce SBPFB, which can significantly improve the SNR of the modulations with discrete TVSF, such as SFBOC and FHBOC. However, we have demonstrated that, when SBPFB is employed, SFBOC receiver has negligible FP loss in the NLOS multipath channels, in contrast to FHBOC receiver that has a large FP loss. As a conclusion, we have demonstrated that the proposed SFBOC is very practical and efficient, and SFBOC can be useful for an advanced signal of the next generation GNSS.

Appendix

In the Appendix, we provide additional performance results for some aspects that are not deeply discussed in the main sections of the paper, such as ZCNM, MSR, ACF output comparison between modulations, discriminator gain, and FOBP.

A. ZCNMs and MSR

To further analyze the correlation property introduced in subsection II-B, we calculate the zero crossings nearest the main peak (ZCNM) and ACF main-peak-to-maximum-side-peak ratio (MSR) [21] as

$$\mathrm{ZCNM} = \pm T_c \times \left(2\left(m_h + m_l\right) - n\right)^{-1}, \tag{58}$$

$$\mathrm{MSR} = 10\log\left(\max_{|\tau|>\tau_{\mathrm{ZCNM}}} |R(\tau)|\right), \tag{59}$$

where τ_{ZCNM} and $R(\tau)$ denote the time delay corresponding to the ZCNM and the ACF output, respectively. We show the MSR and the absolute value of ZCNM for SFBOC(m_h:-1:1,1) for $m_h = \{1, 2, \ldots 60\}$ in Fig. 18. As shown, ZCNM decreases and MSR increases when m_h increases, which agrees with the observation that the main lobe of ACF output becomes narrower and the magnitude of side peaks becomes smaller as found in Fig. 2. For $m_h \leq 20$, ZCNM sharply decreases down to about 0.15 μs and MSR increases up above 15dB, whereas for $m_h > 20$, ZCNM and MSR maintain their tendency but the change becomes smaller. This means that, in SFBOC, the correlation property is continuously improved as

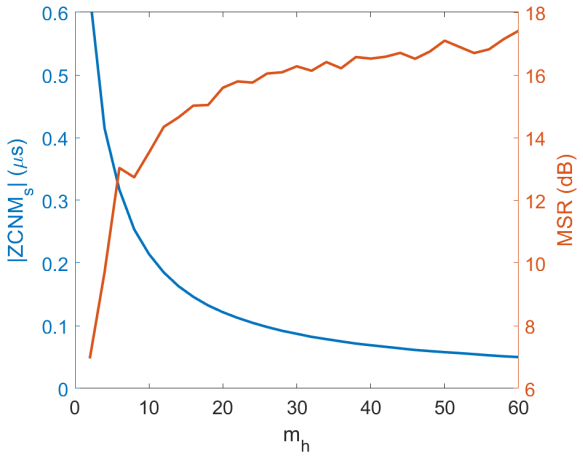

Fig. 18. ZCNM and MSR for SFBOC with $T_c = T_0$.

m_h increases, and, therefore, we can choose the maximum m_h allowed within the given bandwidth to maximize the SFBOC performance.

B. ACF outputs of SFBOC and modulations with TVSF

Fig. 19 shows the ACF outputs of SFBOC(6:-1:1,1), GBOC(6,1,0), and FHBOC(6:1:1,1). As shown, for $|\tau| < 0.3T_c$, SFBOC(6:-1:1,1) and FHBOC(6:1:1,1) have a smaller side peaks but slightly wider main lobe than GBOC(6,1,0). However, for $|\tau| > 0.3T_c$, the magnitude of the side peaks of SFBOC(6:-1:1,1) and FHBOC(6:1:1,1) are slightly larger than that of GBOC(6,1,0). In overall, the difference in the main lobe width and side peak magnitude of the three modulations in the figure are small, when compared to the conventional GNSS modulations shown in Fig. 3. Since the difference in ACF output of the three modulations is small, range accuracy and tracking performance can be similar as discussed in section III-C-E.

C. Discriminator gain

In this subsection, the EL Discriminator output discussed in subsection III-D is analyzed numerically. The slope of the discriminator output at the zero path delay error $\epsilon = 0$, which is the EL discriminator gain G_D [40], is defined as

$$G_D \equiv \left.\frac{dD(\epsilon)}{d\epsilon}\right|_{\epsilon=0}, \tag{60}$$

where $D(\epsilon)$ (31) indicates the discriminator output. Fig. 20 shows the discriminator gain G_D with respect to the early-late correlator spacing Δ for SFBOC(6:-1:1,1) and all compared modulations. As shown, all of the considered modulations except BOC(6,1) have decreasing G_D as Δ increases from 0 to $0.25T_c$. BPSK(1) and BOC(1,1) have small and slowly decreasing G_D, whereas BOC(6,1) has the highest gain among the considered modulations for about $\Delta < 0.05\ T_c$. However, for $\Delta > 0.07T_c$, BOC(6,1) has a negative G_D continuously dropping due to the large side peaks as shown in Fig. 9, which may result in a large tracking ambiguity. On the other

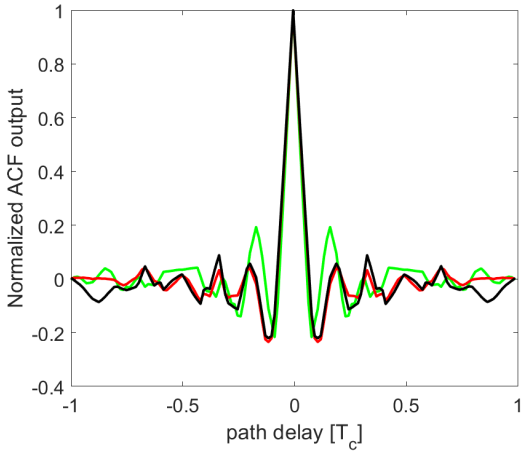

(a) ACF outputs

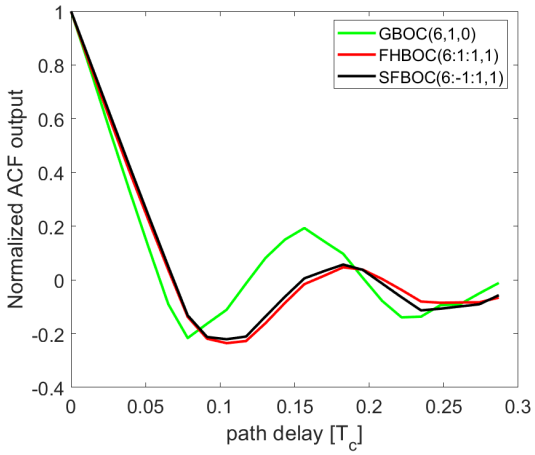

(b) Zoom of ACF outputs

Fig. 19. Normalized ACF outputs for SFBOC(6:-1:1,1), GBOC(6,1,0), and FHBOC(6:1:1,1).

hand, GBOC(6,1,0) shows high G_D similar to BOC(6,1) but its G_D decreases rapidly down to 0 at about $\Delta = 0.07T_c$. SFBOC(6:-1:1,1) and FHBOC(6:1:1,1) has the same strong G_D for all Δ shown in the figure; the maximum G_D is lower than GBOC(6,1,0) but much higher than BPSK(1), BOC(1,1), and CBOC(6,1,1/11), and the G_D decreases down to 0 at about $\Delta = 0.14T_c$. Consequently, SFBOC(6:-1:1,1) shows the same code discriminator performance to FHBOC(6:1:1,1), and the code discriminator performance of SFBOC(6:-1:1,1) is inferior to GBOC(6,1,0) but superior to the conventional GNSS modulations.

D. Fractional Out-of-Band Power

Fractional Out-of-Band Power (FOBP) is a standard metric of spectral containment for digital data. In practice, FOBP can represent the bandwidth efficiency of the signal [41], [42] and is defined as

$$\text{FOBP} = \frac{\int_{BW_o}^{\infty} G_{SF}(f)df}{\int_{0}^{\infty} G_{SF}(f)df}, \tag{61}$$

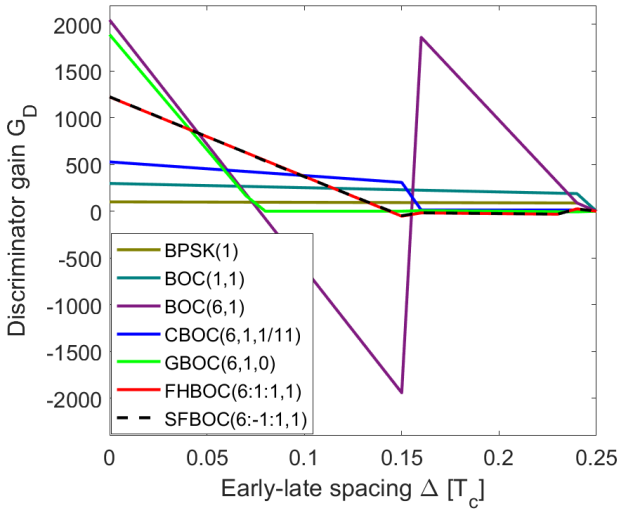

Fig. 20. Discriminator gain G_D for SFBOC(6:-1:1,1) and all compared modulations with unlimited bandwidth.

where BW_o is the single-sideband bandwidth, and $G_{SF}(f)$ (16) is the PSD of SFBOC. Fig. 21 shows the FOBP for various SFBOCs, where SFBOC(11:-1:1,1) and SFBOC(11:-2:1,1) have the highest m_h and the highest FOBP for about $BW_o \leq 12MHz$, but there is a sudden drop below -27dB for about $BW_0 \geq 16MHz$. On the other hand, SFBOC(3:-2:1,1) has the lowest m_h, and the smallest FOBP for all BW_o. Therefore, we conclude that, when $i_m = 1$, bandwidth efficiency improves as the bandwidth and m_h increase.

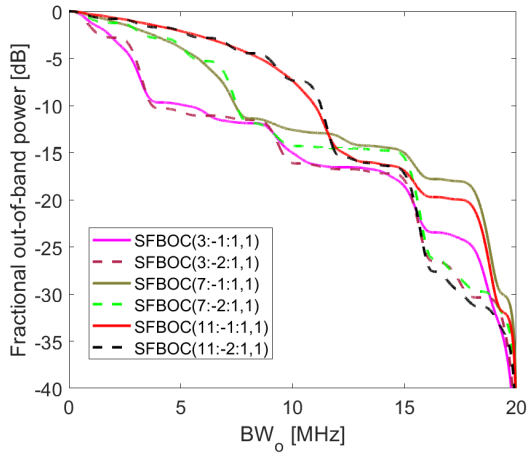

Fig. 21. FOBP for various SFBOCs.

E. Sampling Timing Offset

In order to analyze the correlation loss due to the sampling timing offset (STO) of SFBOC, we compare the correlation loss of BOC(m_k,1) ($m_k = \{1, 2 \ldots 6\}$), since BOC(m_k,1) is the base modulation of SFBOC(6:-1:1,1). STO is a random sampling time offset between the first sample point and the starting point of the chip, and the BOC(m_k,1) subcarrier has

the same number of +1's and -1's within one subcarrier period T_{sc}. Therefore, to avoid any correlation loss due to the STO,

$$N_{SPC} \bmod 2m_k = 0 \tag{62}$$

should be satisfied, where '$a \bmod b$' is the remainder when b divides a, N_{SPC} $(= f_s T_c)$ is the number of samples per chip.

Fig. 22 shows the correlation loss of BOC(m_k,1) for $m_k \in \{1, 2, \dots 6\}$, code Doppler frequency $|f_{cd}| \leq 6.5$Hz, and sampling frequency $f_s = 12f_0$, $24f_0$, and $120f_0$. Note that the sampling frequency f_s $(= 120f_0)$ satisfies (62) for all $m_k = \{1, 2, \dots 6\}$, so that the correlation loss due to the STO does not occur. Fig. 22 shows average correlation loss of BOC(m_k,1) for $m_k \in \{1, 2, \dots 6\}$ and $T_{corr} = 1, 5, 10$[ms] with respect to the code Doppler f_{cd}, for various sampling frequencies f_s $(= 120f_o, 24f_o$, and $12f_o)$. The average correlation loss is calculated from the average correlation loss of the 100 randomly selected STOs in $[0, T_s)$. As shown, the correlation loss generally increases with the increase of $|f_{cd}|$ and m_k. Since the sampling rate $f_s = 12f_0$ (i.e., $N_{SPC} = 12$) in Fig. 22a does not satisfy (62) for BOC(4,1) and BOC(5,1), the correlation loss of about 21% and 35% occurs due to the STO, respectively, even without the code-Doppler (i.e., $f_{cd} = 0$). In Fig. 22b, all of the BOC(m_k,1) signals has correlation loss for $m_k \in \{1, 2, \dots 6\}$ due to the f_{cd}, which is similar to the results in Fig. 22a. However, BOC(5,1) is the only one that does not satisfy (62) for $f_s = 24f_0$, and shows correlation loss of about 19% due to the STO. In Fig. 22c, since all BOC signals satisfy (62), there is only correlation loss due to the f_{cd}(40) shown in the figure.

Note that, in the case of GBOC, the subcarrier frequency is continuously changing, so that GBOC cannot satisfy (62) for any f_s and the correlation loss due to the STO always occurs, as discussed in subsection III-F. Note also that, based on the results shown in Fig. 22c, we can find the difference in the correlation loss for increasing or decreasing $M_k(t)$ (7) of SFBOC. As shown, higher f_{sc} and longer T_{corr} cause larger companding of the BOC signal, and the correlation loss is decreasing linearly. That means, BOC(m_k,1) with larger m_k suffers more from the signal companding as T_{corr} increases, and that BOC(m_k,1) with smaller m_k suffers (slightly) less than larger m_k, when T_{corr} increases. In case of SFBOC with decreasing subcarrier frequency, BOC signals with higher subcarrier frequency f_{sc} occurs earlier than the BOC signals with lower subcarrier frequency within the T_{code}. As a result, SFBOC with decreasing $M_k(t)$ shows slight advantage over SFBOC with increasing $M_k(t)$, regardless of the starting point of correlation, as shown in Fig. 22d.

ACKNOWLEDGEMENT

This work was supported by Electronics and Telecommunication Research Institute (ETRI) (21ZH1100, Study on 3D Communication Technology for Hyper-Connectivity), and the National Research Foundation of Korea(NRF) grant funded by the Korea government(MSIT) (No. 2021R1A2C3008370), .

REFERENCES

[1] J. W. Betz and K. R. Kolodziejski, "Generalized theory of code tracking with an early-late discriminator part II: Noncoherent processing and numerical results," *IEEE Transactions on Aerospace and Electronic Systems*, vol. 45, no. 4, pp. 1557–1564, 2009.

[2] D. Torrieri, *Principles of spread-spectrum communication systems*. Berlin, Heidelberg, Germany: Springer, 2005.

[3] C. Hegarty, J. W. Betz, and A. Saidi, "Binary coded symbol modulations for gnss," in *Proceedings of the 60th Annual Meeting of The Institute of Navigation (2004)*, 2004, pp. 56–64.

[4] J. W. Betz, "Binary offset carrier modulations for radionavigation," *Navigation*, vol. 48, no. 4, pp. 227–246, 2001.

[5] G. W. Hein, J.-A. Avila-Rodriguez, S. Wallner, A. R. Pratt, J. Owen, J.-L. Issler, J. W. Betz, C. J. Hegarty, S. Lenahan, J. J. Rushanan *et al.*, "MBOC: the new optimized spreading modulation recommended for GALILEO L1 OS and GPS L1C," in *Proceedings of IEEE/ION PLANS 2006*, 2006, pp. 883–892.

[6] J. W. Betz, "The offset carrier modulation for GPS modernization," in *Proceedings of the 1999 National Technical Meeting of The Institute of Navigation*, 1999, pp. 639–648.

[7] Z. Yao, X. Cui, M. Lu, Z. Feng, and J. Yang, "Pseudo-correlation-function-based unambiguous tracking technique for sine-BOC signals," *IEEE Transactions on Aerospace and Electronic Systems*, vol. 46, no. 4, pp. 1782–1796, 2010.

[8] P. W. Ward and W. E. Lillo, "Ambiguity removal method for any gnss binary offset carrier (BOC) modulation," in *Proceedings of the 2009 International Technical Meeting of The Institute of Navigation*, 2009, pp. 406–419.

[9] V. Heiries, D. Roviras, L. Ries, and V. Calmettes, "Analysis of non ambiguous BOC signal acquisition performance," in *Proceedings of the 17th International Technical Meeting of the Satellite Division of the Institute of Navigation (ION GNSS 2004)*, 2004, pp. 2611–2622.

[10] O. Julien, C. Macabiau, M. E. Cannon, and G. Lachapelle, "Aspect: unambiguous sine-BOC (n, n) acquisition/tracking technique for navigation applications," *IEEE Transactions on Aerospace and Electronic Systems*, vol. 43, no. 1, pp. 150–162, 2007.

[11] H. Ko, B. Kim, and S.-H. Kong, "GNSS multipath-resistant cooperative navigation in urban vehicular networks," *IEEE Transactions on Vehicular Technology*, vol. 64, no. 12, pp. 5450–5463, 2015.

[12] S.-H. Kong, "Statistical analysis of urban GPS multipaths and pseudo-range measurement errors," *IEEE transactions on aerospace and electronic systems*, vol. 47, no. 2, pp. 1101–1113, 2011.

[13] S. M. Kay, *Fundamentals of statistical signal processing: estimation theory*. Hoboken, NJ, USA: Prentice-Hall, Inc., 1993.

[14] J. W. Betz and K. R. Kolodziejski, "Generalized theory of code tracking with an early-late discriminator part II: Noncoherent processing and numerical results," *IEEE Transactions on Aerospace and Electronic Systems*, vol. 45, no. 4, pp. 1557–1564, 2009.

[15] P. Fine and W. Wilson, "Tracking algorithm for GPS offset carrier signals," in *Proceedings of the 1999 national technical meeting of The Institute of Navigation*, 1999, pp. 671–676.

[16] G. W. Hein, J.-A. Avila-Rodriguez, L. Ries, L. Lestarquit, J.-L. Issler, J. Godet, and T. Pratt, "A candidate for the GALILEO l1 OS optimized signal," in *proceedings of the 18th international technical meeting of the satellite division of the institute of navigation (ION GNSS 2005)*, 2005, pp. 833–845.

[17] Z. Yao and M. Lu, *Next-Generation GNSS Signal Design*. Berlin, Heidelberg, Germany: Springer, 2021.

[18] F. Dovis, *GNSS interference threats and countermeasures*. Norwood, MA, USA: Artech House, 2015.

[19] F. D. Nunes, J. M. Leitao, and F. M. Sousa, "Performance analysis of an absolute phase modulation scheme for GNSS signals," in *2016 8th ESA Workshop on Satellite Navigation Technologies and European Workshop on GNSS Signals and Signal Processing (NAVITEC)*. IEEE, 2016, pp. 1–8.

[20] F. D. Nunes, F. M. Sousa, and J. Leitão, "Characterization and performance analysis of generalized BOC modulations for GNSS," *NAVIGATION, Journal of the Institute of Navigation*, vol. 66, no. 1, pp. 185–197, 2019.

[21] J. Ma, Y. Yang, H. Li, and J. Li, "FH-BOC: generalized low-ambiguity anti-interference spread spectrum modulation based on frequency-hopping binary offset carrier," *GPS Solutions*, vol. 24, no. 3, pp. 1–16, 2020.

[22] D. A. Noon, "Stepped-frequency radar design and signal processing enhances ground penetrating radar performance," Ph.D. dissertation,

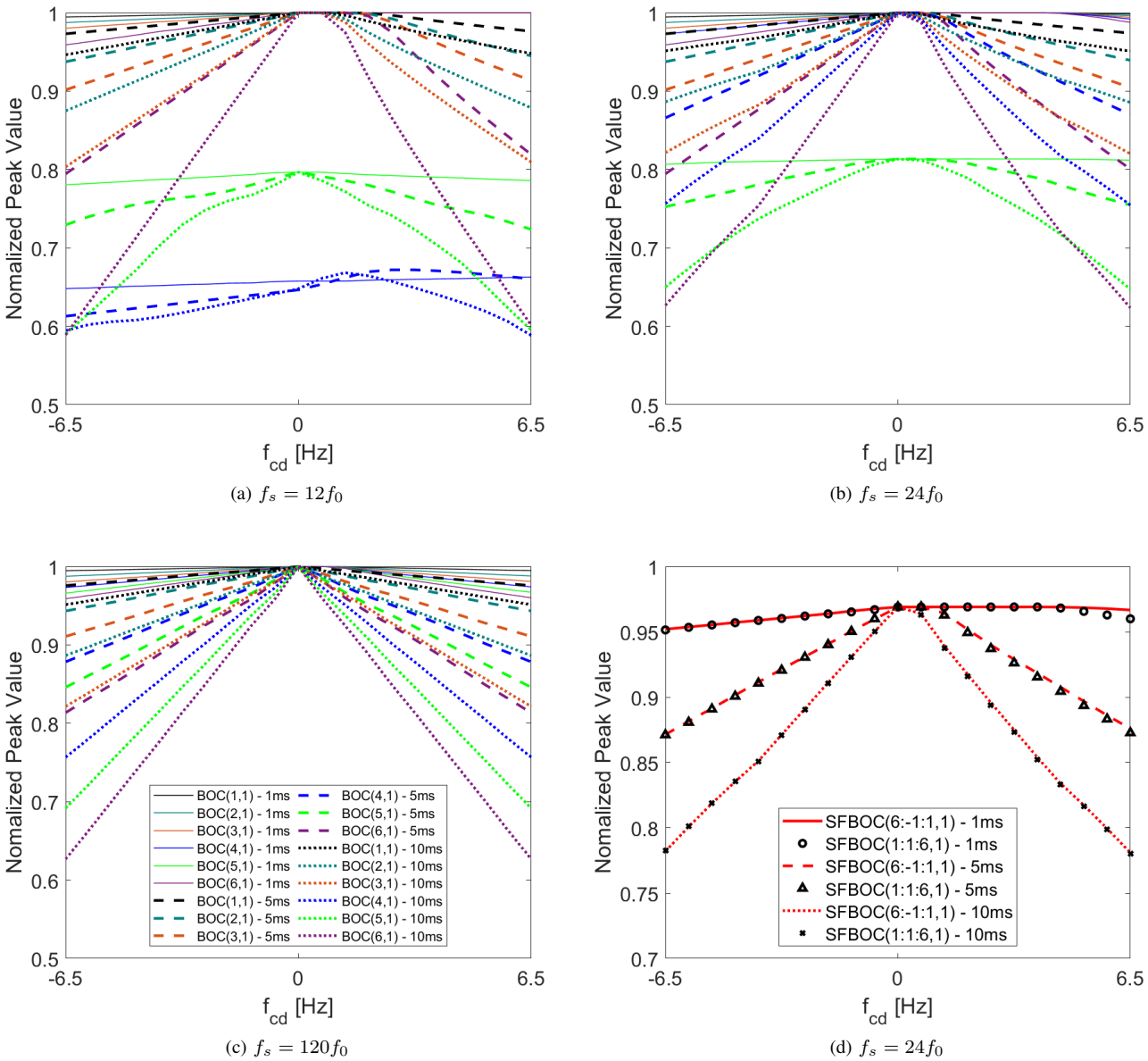

(a) $f_s = 12f_0$ (b) $f_s = 24f_0$

(c) $f_s = 120f_0$ (d) $f_s = 24f_0$

Fig. 22. BOC and SFBOC correlation losses for various sampling frequencies and correlation intervals.

Dept. Electr. Comput. Eng., Univ. Queensland, Brisbane, Australia, 1996.

[23] C. Nguyen and J. Park, *Stepped-Frequency Radar Sensors: Theory, Analysis and Design*. Berlin, Heidelberg, Germany: Springer, 2016.

[24] J. W. Betz, "On the power spectral density of GNSS signals, with applications," in *Proceedings of the 2010 International Technical Meeting of the Institute of Navigation*, 2010, pp. 859–871.

[25] S. S. I. On, *Digital communications*. New York, NY, USA: Van Nostrand Reinhold, 1985.

[26] F. M. Sousa and F. D. Nunes, "New expressions for the autocorrelation function of BOC GNSS signals," *NAVIGATION, Journal of the Institute of Navigation*, vol. 60, no. 1, pp. 1–9, 2013.

[27] O. Julien, M. E. Cannon, G. Lachapelle, C. Mongrédien, and C. Macabiau, "A new unambiguous BOC (n, n) signal tracking technique," in *Proceedings of The European Navigation Conference GNSS*, 2004, pp. 17–19.

[28] P. M. Fishman and J. W. Betz, "Predicting performance of direct acquisition for the M-code signal," in *Proceedings of the 2000 national technical meeting of the institute of navigation*, 2000, pp. 574–582.

[29] N. Wiener *et al.*, *Extrapolation, interpolation, and smoothing of stationary time series: with engineering applications*. Cambridge, MA, USA: MIT press, 1964, vol. 8.

[30] J.-L. Issler, L. Ries, L. Lestarquit, O. Nouvel, and Q. Jeandel, "Spectral measurements of GNSS satellite signals need for wide transmitted bands," in *Proceedings of the 16th International Technical Meeting of the Satellite Division of The Institute of Navigation (ION GPS/GNSS 2003)*, 2003, pp. 445–460.

[31] M. Irsigler, J. A. Avila-Rodriguez, and G. W. Hein, "Criteria for GNSS multipath performance assessment," in *Proceedings of the 18th International Technical Meeting of the Satellite Division of The Institute of Navigation (ION GNSS 2005)*, 2005, pp. 2166–2177.

[32] R. Pickholtz, D. Schilling, and L. Milstein, "Theory of spread-spectrum communications-a tutorial," *IEEE transactions on Communications*, vol. 30, no. 5, pp. 855–884, 1982.

[33] S. M. Kay, *Fundamentals of statistical signal processing: estimation theory*. Hoboken, NJ, USA: Prentice-Hall, Inc., 1993.

[34] J. J. Spilker Jr, P. Axelrad, B. W. Parkinson, and P. Enge, *Global positioning system: theory and applications, volume I*. Reston, VA, USA: American Institute of Aeronautics and Astronautics, 1996.

[35] P. Misra and P. Enge, *Global Positioning System: Signals, Measurements, and Performance*. Lincoln, MA, USA: Ganga-Jamuna Press, 2011.

[36] A. N. Akansu, R. A. Haddad, and P. A. Haddad, *Multiresolution signal decomposition: transforms, subbands, and wavelets*. Cambridge, MA, USA: Academic press, 2001.

[37] N. Harper, *Server-side GPS and Assisted-GPS in Java*. Norwood, MA, USA: Artech House, 2010.

[38] T. Ren and M. G. Petovello, "A stand-alone approach for high-sensitivity GNSS receivers in signal-challenged environment," *IEEE Transactions on Aerospace and Electronic Systems*, vol. 53, no. 5, pp. 2438–2448, 2017.

[39] S.-H. Kong, S. Cho, and E. Kim, "GPS first path detection network based on MLP-Mixers," *IEEE Transactions on Wireless Communications*, 2022.

[40] J. W. Betz, "Design and performance of code tracking for the GPS m code signal," in *Proceedings of the 13th International Technical Meeting of the Satellite Division of The Institute of Navigation (ION GPS 2000)*, 2000, pp. 2140–2150.

[41] F. Amoroso, "Fractional out-of-band power formulas for BPSK, QPSK and MSK," *Channels*, vol. 5, p. 6G, 2000.

[42] I. Ghareeb, "Bit error rate performance and power spectral density of a noncoherent hybrid frequency-phase modulation system," *IEEE journal on selected areas in communications*, vol. 13, no. 2, pp. 276–284, 1995.

Seung-Hyun Kong (M'06–SM'16) is an Associate Professor in Graduate School of Mobility of Korea Advanced Institute of Science and Technology (KAIST), where he has been a faculty member since 2010. He received a B.S. degree in Electronics Engineering from Sogang University, Seoul, Korea, in 1992, an M.S. degree in Electrical and Computer Engineering from Polytechnic University (merged to NYU), New York, in 1994, a Ph.D. degree in Aeronautics and Astronautics from Stanford University, Palo Alto, in 2005. From 1997 to 2004 and from 2006 to 2010, he was with companies including Samsung Electronics (Telecommunication Research Center), Korea, and Qualcomm (Corporate R&D Department), San Diego, USA for advanced technology R&D in mobile communication systems, wireless positioning, and assisted GNSS. Since he joined KAIST as a faculty member in 2010, he has been working on various R&D projects in advanced intelligent transportation systems, such as robust GNSS-based navigation for urban environment, deep learning and reinforcement learning algorithms for autonomous vehicles, sensor fusion, and vehicular communication systems (V2X). He has authored more than 100 papers in peer-reviewed journals and conference proceedings and 12 patents, and his research group won the President Award (of Korea) in the 2018 international student autonomous driving competition host by the Korean government. He has served as an associate editor of IEEE T-ITS and IEEE Access, an editor of IET-RSN and the lead guest editor of the IEEE TITS special issue on "ITS empowered by AI technologie" and the IEEE Access special section on "GNSS, Localization, and Navigation Technologies". He has served as the program chair of IPNT from 2017 to 2019 in Korea and as a program co-chair of IEEE ITSC2019, New Zealand

Sangjae Cho received the B.S. degree in Department of Energy and Electrical Engineering from Korea Polytechnic University, Korea, in 2018 and M.S. degree in Graduate School of Mobility from Korea Advanced Institute of Science and Technology (KAIST), where he is currently pursuing the Ph.D. degree. His research interests include GNSS, Signal processing, Deep learning, Autonomous vehicle, and Wireless communication.

Taeseon Kim received the B.S. degree in Electronics Engineering from Hanbat University, Korea, in 2010. He is currently a Research Associate of the Autonomous Vehicles and Electronics laboratory, Graduate School of Mobility, Korea Advanced Institute of Science and Technology (KAIST). His research interests include GNSS, and Autonomous vehicle.

Sanguk Lee received the BS from Yonsei University, Seoul, Korea, in 1988 and the MS and PhD degrees in aerospace engineering from Auburn University, Alabama, U.S.A in 1991 and 1994, respectively. He has been principal researcher at Electronics Telecommunications Research Institute (ETRI) since 1993 and is leader of KPS satellite navigation research center. He developed satellite SW simulators for KOREASAT-1, KOMPSAT-1, KOMPSAT-2, and COMS-1. And he developed GNSS ground station system and SAR distress beacon Technologies development, GPS interference monitoring, localization and mitigation, GNSS interference detection, localization by UAV as project manager. His research interests are satellite control, satellite & GNSS modeling and simulation, GNSS system and applications and so on.